2015

Functional Characterization of rai1 in Zebrafish

Joshua S. Beach
Virginia Commonwealth University, beachjs@vcu.edu

FUNCTIONAL CHARACTERIZATION OF RAI1 IN ZEBRAFISH

A thesis submitted in partial fulfillment of the requirements for the degree of Master of Science
at Virginia Commonwealth University
by

JOSHUA SHAY BEACH
Bachelor of Biology
Belmont Abbey College, 2011

DIRECTOR: DR. JAMES A. LISTER
Assistant Professor, Department of Human and Molecular Genetics

Virginia Commonwealth University
Richmond, VA
April, 2015

Acknowledgement

First and foremost, I want to thank everyone who has supported and motivated me throughout my graduate studies, without you I don't think I would be finishing today. I had the distinct privilege of working for Dr. James Lister, an amazing mentor and a great man. His unwavering patience and guidance helped me through countless failed experiments and I cannot thank him enough for such wonderful support. I want to thank the rest of the Lister lab members for their support and great company. The laughs and troubleshooting advice were greatly appreciated during the ups and downs of this project.

I would like to thank Dr. Sarah Elsea for her guidance and support during my first rotation. Her ability to dissect a technical problem was remarkable and I have tried to bring that mindset on into my work. I would also thank the Elsea lab for their guidance and the support during my first months in the graduate program. I would also like to thank Dr. Rita Shiang for her support as a committee member, providing excellent guidance and feedback for my project.

Finally, I would like to thank my mother, sister, grandparents, and the rest of my friends and loved ones for their unending support during these past three years.

Table of Contents

Table of Contents Page

List of Figures

Page

Abstract

FUNCTIONAL CHARACTERIZATION OF *RAI1* IN ZEBRAFISH

By Joshua Shay Beach, B.A.

A Thesis submitted in partial fulfillment of the requirements for the degree of Master of Science at Virginia Commonwealth University.

Virginia Commonwealth University, 2015

Major Director: Dr. James A. Lister

Assistant Professor, Department of Human and Molecular Genetics

Smith-Magenis Syndrome (SMS; OMIM #182290) is a multiple congenital abnormality and intellectual disability (ID) disorder caused by either an interstitial deletion of the 17p11.2 region containing the retinoic acid induced-1 (*RAI1*) gene or a mutation of the *RAI1* gene. Individuals diagnosed with SMS typically present characteristics such as ID, self-injurious behavior, sleep

disturbance, ocular and otolaryngological abnormalities, craniofacial and skeletal abnormalities, neurological and behavioral abnormalities, as well as other systemic defects and manifestations. Previous work by Vyas in 2009 showed temporal expression of *rai1* in zebrafish embryos as early as 9 hpf. We hypothesize that there is maternal *rai1* expression as early as zero hours post fertilization in wild type embryos. Using end-point PCR, we found that in fact there is maternal *rai1* expression is detectable as early as 2 hours post fertilization (hpf) in wild type zebrafish embryos. Furthermore, we quantified *rai1* expression using qPCR and found that *rai1* expression declines significantly after 6 hpf. We hypothesize that a down regulation of *rai1* or loss of *rai1* will lead to morphological phenotypes, especially if that loss of *rai1* function occurs during the earliest stages of zebrafish embryogenesis. Using a *rai1*morpholino oligonucleotide (MO), we found a loss of *rai1* expression did not induce a morphological phenotype in in wild type embryos; furthermore, we also found that a loss of maternal *rai1* expression did not induce a morphological phenotype as well. Utilizing a mutant *rai1* zebrafish line, we found that both *rai1 +/fh370* progeny nor *rai1 fh370/fh370* progeny exhibited a morphological phenotype and that downstream targets such as *bdnf* were not affected by a reduction or complete loss of *rai1*. Prior research has shown that retinoic acid (RA) can induce *rai1* expression. We hypothesize that RA can induce expression of *rai1* during zebrafish embryogenesis. Using wild type fish and a *rai1 in situ* hybridization probe, we found that RA treatment at 25 hpf induced expression of *rai1*. The construction of a *rai1* overexpression vector used for overexpression studies was started. Further development of GFP expression vector and zebrafish rai1 antibody are needed to determine if the morpholino is reducing *rai1* protein expression.

CHAPTER 1: Introduction

Smith-Magenis syndrome

Smith-Magenis Syndrome (SMS; OMIM #182290) is a multiple congenital abnormalities and intellectual disability (ID) disorder caused by either an interstitial deletion of the 17p11.2 region containing the retinoic acid induced-1 (*RAI1*) gene or a mutation of the *RAI1* gene. Patients diagnosed with SMS typically present characteristics such as ID, self-injurious behavior, sleep disturbance, ocular and otolaryngological abnormalities, craniofacial and skeletal abnormalities, neurological and behavioral abnormalities, as well as other systemic defects and manifestations. Ann Smith and Ellen Magenis reported the first SMS patients in 1986 (Smith et al.). The 17p11.2 deletion was detected through the use of the standard Giesma staining (G-banding) technique (Smith et al. 1986). Initially, SMS was believed to be a contiguous gene syndrome with the 17p11.2 deletion spanning approximately 80 genes (Smith et al. 1986). The development of fluorescent *in-situ* hybridization (FISH) gave investigators a more effective tool for identifying the deletion, as FISH also allowed mapping of deletions of various sizes on the 17p11.2 region, redefining the SMS critical region to approximately 700 kb (Vlangos et al. 2004). Approximately 90% of SMS patients have a FISH detectable 17p11.2 microdeletion ranging from 1.5 to approximately 9 Mb, while the remaining 10% of SMS patients have

mutations in the *RAI1* gene (Elsea and Girirajan 2008). As technology improved, the development of multiplex ligation-dependent probe amplification (MLPA), array comparative genomic hybridization (aCGH), and real-time quantitative PCR (qPCR) allowed investigators to identify even smaller deletions (Kriek et al. 2007; Williams et al. 2010; Truong et al. 2008). An estimated 70 – 75% of SMS patients with 17p11.2 deletions possess a "common" deletion of 3.7 Mb, while the remaining 25 – 30% contain larger or smaller deletions (Elsea and Girirajan 2008; Vlangos et al. 2004). Typically, SMS cases are sporadic throughout populations (Elsea and Girirajan 2008). The prevalence of SMS is believed to be between 1:15,000 and 1:25,000; however, these are conservative estimates with a much greater expected occurrence due to many individuals with SMS not being diagnosed.

Ocular/Otolaryngological Abnormalities

Ocular abnormalities observed in SMS patients at a high frequency include strabismus, degenerative myopia, and microcornea (Barnicoat et al. 1996; Chen et al. 1996; Finucane et al. 1993). SMS patients also presented no definable iris collarette, stromal dysplasia, nasal correctopia, Wölfflin-Kruckmann spots, dysplastic optic nerves, iris dysgenesis, and colobomas (Barnicoat et al. 1996; Chen et al. 1996; Finucane et al. 1993; Greenberg et al. 1996). Figure 1A and 1B illustrate the presence of prominent Wölfflin-Kruckmann spots, slight nasal correctopia, poorly defined or absent collarette, and altered anterior stromal texture (Chen et al. 1996). In the study conducted by Finucane and colleagues, three of the ten patients ophthalmologically evaluated presented with retinal detachment (1993). It was noted that the retinal detachments did not occur because of a morphological phenotype within the eye due to the17p11.2 deletion. Instead, two of the three SMS patients had detached retinas due to self-injurious behavior, while

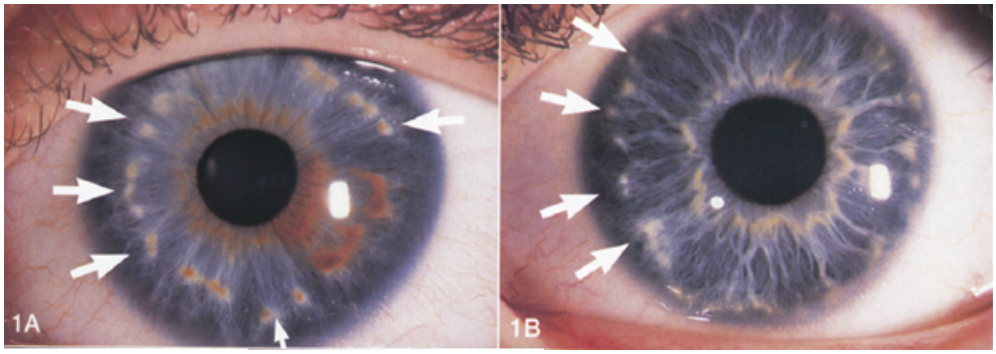

Figure 1. **Images showing iris anomalies in Smith-Magenis syndrome patients.** (A) Left iris of a l2 year-old girl; (B), right iris of a 15-year-old boy. Notice slight nasal correctopia, poorly defined or absent collarette, altered anterior stromal texture, and prominent Wölfflin-Kruckmann spots (arrows).

Source: (Chen et al 1996).

the third SMS patient had a non-traumatic retinal detachment. However, the authors maintain that there is a strong association of moderate to high retinal detachment in Smith-Magenis syndrome patients (Finucane and Jaeger 1997).

Individuals with Smith-Magenis syndrome are also observed to have otolaryngological anomalies. A multidisciplinary study found that 94% percent of SMS patients (n = 17) presented with abnormal otolaryngological phenotypes such as conductive hearing impairment typically in the mild range, sensorineural hearing loss, hoarse voice, throat polyps, nodules, edema, or paralysis (Greenberg et al. 1996). In a case study conducted by Di Cicco and colleagues, an ear and sinus CT scan of a 9 year old SMS patient showed chronic otitis media with effusion (OME), mastoiditis with left erosion of ossicular bones, and an uneven maxillary sinus floor compared to the nasal floor (Figure 2) (2001). Liburd and colleagues investigated the myosin XVA (*MYO15A*) gene, involved with hearing loss, in 8 SMS patients (2001). The *MYO15A* gene is located in the 17p11.2 region and the one SMS common deletion patient with severe hearing loss possessed one copy of *MYO15A*, with a mutation in this non-deleted *MYO15A* allele (Figure 3), allowing for expression of this recessive phenotype.

Craniofacial/Skeletal Abnormalities

Diagnosed SMS patients present an array of craniofacial and developmental dental anomalies (Tomona et al. 2006). Dental anomalies of SMS patients include taurodontism, microdontia, dilacerations of molars and canines, and tooth agenesis. Tooth agenesis and taurodontism are the most common dental anomalies with both anomalies found in 86% of 15 SMS patients screened (Figure 4). Poor gingival health and an increased presence of decayed and filled teeth were also observed in SMS patients. SMS patient dental caries had decayed and filled

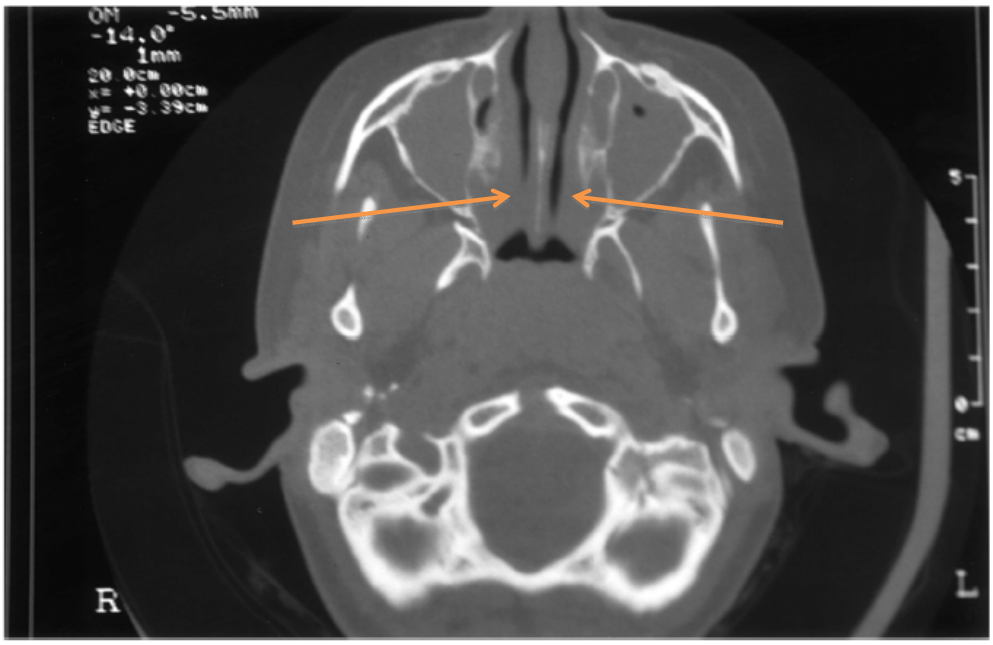

Figure 2. Ear and sinus CT scan of 9 year old girl with SMS. The floor of the maxillary cavity is not level with the nasal cavity; there is a presence of chronic otitis media and mastoiditis with left erosion of the ossicular bones.

Source: (Di Cicco et al. 2001)

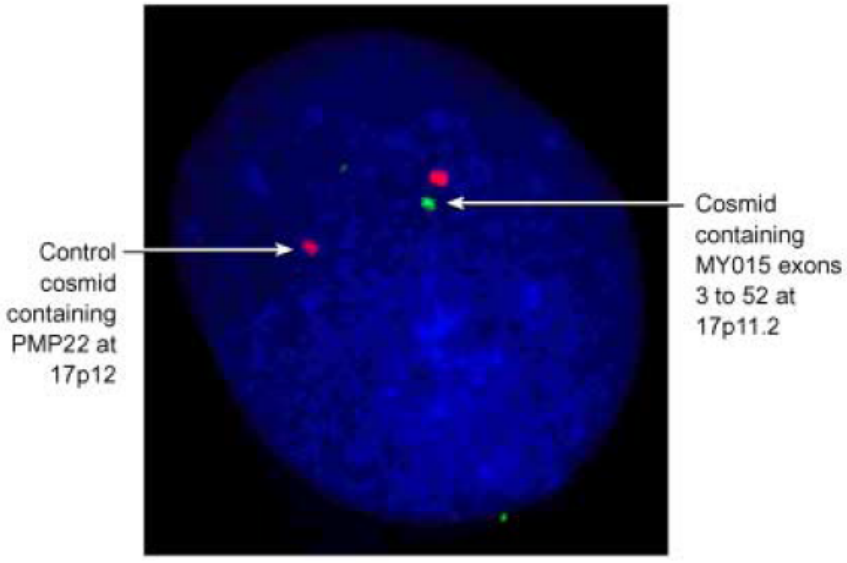

Figure 3. FISH analysis of interphase lymphoblast cells of an SMS patient. The two red signals in the nuclei represent *PMP22*, consistent with the retention of *PMP22* on both chromosomes 17. When the cosmid c155D2, containing exons 3–52 of *MYO15A* was used as a probe, only one copy (*green* signal) of *MYO15A* was observed.

Figure 4. An x-ray image showing dental anomalies in an SMS patient. The arrows illustrate the presence of retained primary molars at the sites of congenitally missing secondary premolars. The presence of taurodont pulps can be observed in the upper permanent molars and lower permanent first molars.

(DFT) scores that were higher than the decayed, missing, and filled teeth (DMFT) ranges reported by the World Health Organization for ages 14 to 19. DMFT scores were not used in the study for SMS patients due to the fact that missing teeth may have been caused by reasons other than for tooth decay. There are distinctive craniofacial anomalies that are present in addition to the dental anomalies. Craniofacial anomalies include brachycephaly, square and protruding jaw with mandibular dimensions greater than maxillary, midface hypoplasia, frontal blossing (pronounced forehead), increased size of the bony chin, abnormal ears, synophrys, tented upper lip, and a short nose with a broad base and full tip (Figure 5) (Allanson et al. 1999; Elsea and Williams 2011; Tomona et al. 2006). As a child ages, the face lengthens and the jaw becomes more square in tandem with heavier brows extending further out laterally than typically found in the normal population (Figure 6; Figure 7) (Allonsen et al. 1999).

SMS patients present numerous skeletal abnormalities which impact their day-to-day functioning and overall quality of life. Skeletal abnormalities include scoliosis, brachydactyly, fifth finger clinodactyly, forearm and elbow limitations, 2/3 toe syndactyly, and polydactyly (Girirajan et al. 2006; Edelman et al. 2007; Elsea and Girirajan 2008; Elsea and Williams 2011; MarianneJensen and Kirchoff 2005). Brachydactyly in an SMS patient is shown in Figure 8 (Elsea and Girirajan 2008). Figure 9 shows the preoperative anterior and lateral views of the spine of an SMS patient with scoliosis showing severe curvature of up to 85 degrees (Tsirikos et al. 2010). Patients typically require reparative surgery to correct the curvature of the spine, in this case by over 40 degrees (Figure 10) (Tsirikos et al. 2010).

Neurological/Behavioral Abnormalities

SMS is most easily recognizable through the identification of neurological and behavioral phenotypes that are unique to this syndrome. While not unique to Smith–Magenis syndrome,

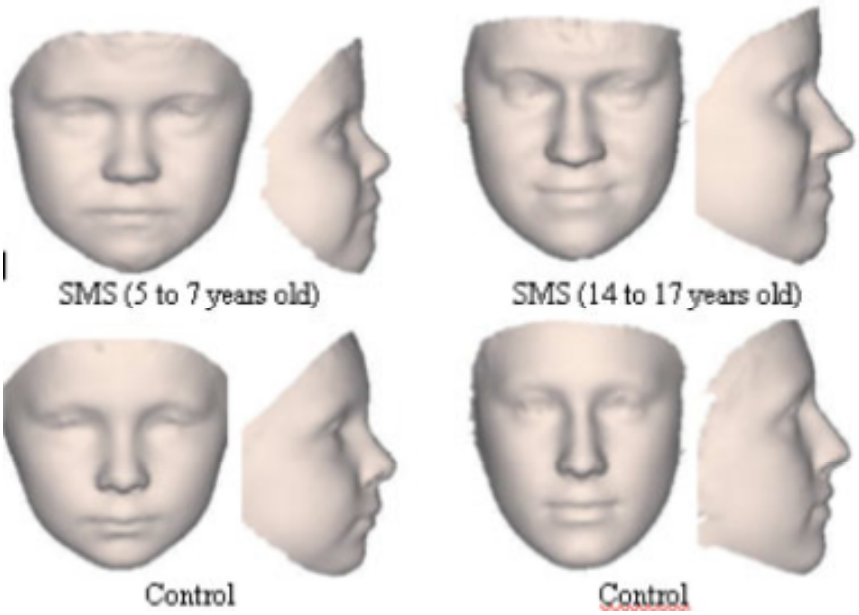

Figure 5. Three dimensional images taken of control and SMS patients' faces shown side by side. Up top, SMS patients exhibit a wide and pronounced mandible with a flat nasal bridge, pointed chin, and flat face when compared to control images.

Source: (Tomona et al. 2006)

Figure 6. Craniofacial development of an SMS patient over the course of 10 years. A & B, 7 months old, note the broad forehead, upslanted palpebral fissures, full-tipped and upturned nose, tented upper lip, and open mouth posture. C, 3 years old, C – D, note the broad and flat nasal bridge, E, mild brachydactyly present, F, 10 years old, full lips and broad nasal bridge.

Source: (Vyas 2009)

Figure 7. Photograph of an adult SMS patient which highlights phenotypes that develop over years. Note the thickened brow that also extends further past the lateral ends of the eye socket when compared to non-SMS individuals; furthermore, the broad nasal bridge and square jaw are more pronounced with age.

Source: (Allanson et al. 1999)

Figure 8. Photograph illustrating brachydactyly in an SMS patient. Note the brachydactyly present in both the hands and feet of an SMS patient. Also observable are nail lesions as well as nail damage from attempted nail pulling.

Source: (Elsea and Girirajan 2008)

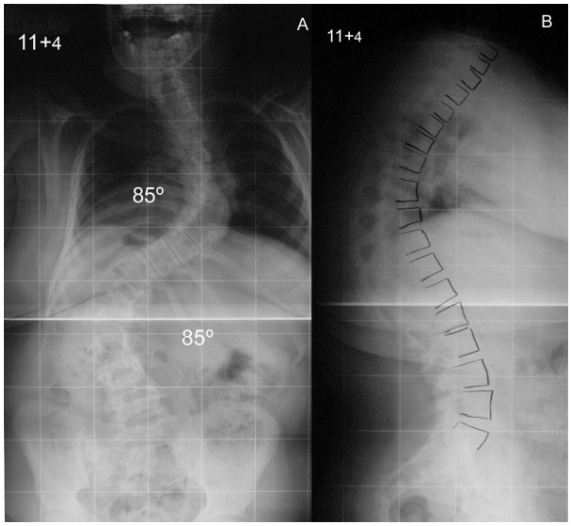

Figure 9. X-ray images of the spine of an SMS patient with severe scoliosis. Note the degrees of angles in the thoracic and lumbar regions, left, anterior view, right, lateral view.

Source: (Tsirikos et al. 2010)

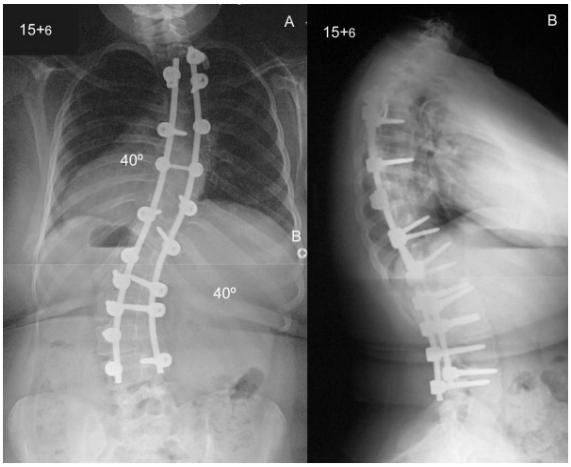

Figure 10. X-ray images of the spine of an SMS patient after corrective surgery. Note the improvement of curvature in the thoracic and lumbar regions, left, anterior view, right, lateral view.

Source: (Tsirikos et al. 2010)

patients have mild to moderate ID with IQ ranging from 20 – 78 (Greenberg et al. 1996). A key factor involved with learning and cognitive function is brain derived neurotrophic factor (*BDNF*), a member of the neurotrophins alongside nerve growth factor (*NGF*) (Henderson 1996). *BDNF* plays an essential role in many aspects of neurodevelopment and learning. BDNF is known to induce the mitogen-activated protein-kinase (MAPK) signaling pathway via synapsin I phosphorylation through the trkB receptor (Gomez-Pinilla et al. 2002; Yamada et al. 2002). This protein-kinase signaling pathway is known to modulate neurotransmitter release. In response to the increases in BDNF, trkB, and synapsin I levels within the spinal cord, there is a rise in *GAP-43* mRNA. GAP-43 plays a role in maintaining synaptic function by promoting axonal growth, learning and memory, and neurotransmitter release. In addition to the rise in *GAP-43* mRNA levels, *CREB* mRNA levels also increases. CREB is required for short and long term memory as well as neuronal resistance to damage. CREB is phosphorylated by BDNF at the transcription regulatory site, and provides a positive feedback loop for transcriptional regulation of BDNF through a calcium-dependent mechanism. BDNF may be an important gene in Smith–Magenis syndrome as directly regulated RAI1 binds to *BDNF* (Burns et al. 2010). Burns and colleagues utilized a chromatin immunoprecipitation – microarray chip (ChIP-chip) to identify genomic sequences bound by RAI1 (2010). With the data from the ChIP-chip, the team found an enhancer element within intron 1 of *BDNF* that was bound by RAI1 (Burns et al. 2010). After attaching the luciferase gene 3' of the enhancer region, the team confirmed a positive regulation of BDNF by RAI1, finding a two fold increase in relative luciferase activity when RAI1 (isoform a) was overexpressed (Burns et al. 2010). RAI1 (isoform c) was used as a negative control, which does not contain a nuclear localization sequence or a plant homeobox domain (PHD) domain. With this direct regulation of *BDNF* expression, one can see the potential impact when an individual is

haploinsufficient for a transcription factor that positively regulates genes involved in learning and neuronal integrity. In addition to ID, SMS patients possess an array of maladaptive issues including self-injurious behavior, attention seeking, hostility, decreased sensitivity to pain, delayed fine motor skills, aggression, anxiety, hyperactivity, over dependency, tantrums, impulsiveness, and balance problems (DeLeerSnyder et al. 2001(A); Shelley and Robertson 2005). Furthermore, SMS patients also demonstrate unique motor behaviors including nail pulling (Figure 8), skin picking (Figure 11), and self-hugging behaviors where the child crosses both arms tightly across their chest, pulling the chin downward and tensing the upper body for several seconds at a time (Elsea and Girirajan 2008; Finucane et al. 1993).

Another important and unique abnormality present in SMS cases is inverted circadian rhythm. SMS patients have an inverted circadian rhythm marked by the highest releases of melatonin, the hormone implicated in the bioregulation of circadian rhythms, during the middle of the day which causes SMS patients to want to sleep (Figure 12) (Potocki et al. 2000A; DeLeerSnyder et al. 2001(A)). DeLeersnyder and others measured SMS patient serum melatonin levels against a control group and correlated tantrums with melatonin rise; furthermore, the team hypothesized that part of the hyperactivity and attention deficit is due to SMS patients struggling against sleep during the day when melatonin levels are highest (DeLeerSnyder et al. 2001(A)). Subcutaneous administration of exogenous human growth hormone (HGH) alleviated early waking symptoms of one SMS patient; however, this is a single case study and only extended the patient's average waking time by 90 minutes (Itoh et al. 2004). Another treatment method for improving sleep and behavioral disturbances with individuals with SMS is the administration of β-blockers in conjunction with melatonin treatments (DeLeersnyder et al. 2001(B), DeLeersnyder 2006).

Figure 11. Photograph showing skin lesions on the arms of an SMS patient. Lesions are present on the arms of an SMS patient due to skin picking.

Source: (Elsea and Girirajan 2008).

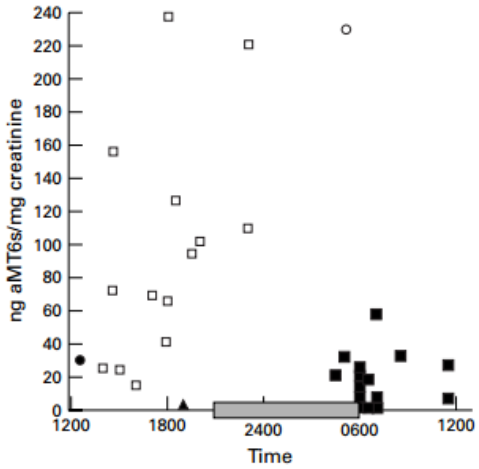

Figure 12. Graph illustrating highest and lowest amounts of secreted melatonin during the day. The peaks (open squares) and troughs (black squares) designate urinary levels of 6-sulphatoxymelatonin. The shaded bar on the x-axis represents typical time of sleep. One case of SMS marked with peaks (open circle) and troughs (black circle) represent values for an SMS patient with an uncommon deletion due to the missing SMS patient specific junction fragment on PFGE. Another case is marked with peak (open triangle) and trough (black triangle), which is an individual with a duplication of the 17p11.2 region.

Source: (Potocki et al. 2000A)

Systemic Defects and Manifestations

Smith – Magenis syndrome patients can exhibit phenotypes that reflect systemic problems. SMS patients typically have a reduction of human growth hormone, which may contribute to their short stature, and in some cases dwarfism (Itoh et al. 2004; Spadoni et al. 2004). SMS patients are also found to present with flat feet, frequent urinary tract infections, undescended testes, hypothyroidism, obesity, hypercholesterolemia, and altered IgA and IgG levels (Elsea and Girirajan 2008; Girirajan et al. 2006). Cardiac anomalies are also known issues with SMS patients; they include cardiomegaly, anomalous pulmonary venous return, mitral valve collapse, tricuspid and mitral regurgitation, aortic stenosis, pulmonary stenosis, tricuspid stenosis, ventricular septal defect (VSD), and atrial septal defects (Elsea and Girirajan 2008; Girirajan et al. 2006).

Potocki-Lupski Syndrome

Potocki-Lupski syndrome (PTLS) is an ID and congenital abnormality syndrome caused by the duplication of the 17p11.2 region, the homologous recombination reciprocal of Smith-Magenis syndrome (Potocki et al. 2000A, Potocki et al. 2000B; Potocki et al. 2007). The duplication ranges in size from as small as 0.41 Mb to as large as 13.3 Mb, with most patients (70-80%) carrying the "common" reciprocal sized duplication of 3.7 Mb (Potocki et al. 2007; Zhang et al. 2010). The smallest region of overlap for these duplications of various sizes spanned the *RAI1* gene (Zhang et al. 2010). Techniques for diagnosing PTLS are similar to that of SMS, as FISH and aCGH are frequently used (Potocki et al. 2000B; Potocki et al. 2007; Zhang et al. 2010). The incidence is much less than when compared to SMS, as duplication syndromes have a milder phenotype compared to deletion syndromes with more than 300 reported SMS cases compared toto ~75 PTLS cases reported (Elsea and Williams 2011; Zhang et al. 2010). There are

fewer PTLS cases because PTLS cases are less likely to be clinically reported compared to SMS (Elsea and Williams 2011; Zhang et al. 2010). Potocki-Lupski syndrome cases are characterized by developmental delay, language impairment, infantile hypotonia, failure to thrive, autistic features, poor neonatal feeding, sleep apnea, EEG abnormalities, oropharyngeal motor dysfunction, cardiovascular abnormalities, and central nervous system (CNS) abnormalities (Potocki et al. 2007) (Soler-Alfonso et al. 2011). However, it must be noted that there have been reported cases of patients without autistic features (Ercan-Senciek et al. 2012; Greco et al. 2008).

Retinoic Acid Induced 1

Role of the *RAI1* gene

Retinoic acid induced 1 (RAI1; OMIM# 607642) is located in the SMS critical region, mapping to the 17p11.2 region (Figure 13) (Bi et al. 2004; Carmona-Mora et al. 2012; Toulouse et al. 2003). *RAI1*is a dosage sensitive gene, as a heterozygous deletion of the gene results in a haploinsufficiency and subsequently causes SMS; in contrast, a duplication of the *RAI1* gene leads to Potocki-Lupski syndrome (Carmona-Mora and Walz 2010; Elsea and Girirajan 2008; Potocki et al. 2005). The *Rai1* gene was first identified as Gt1 in mouse P19 embryonic carcinoma cells where its expression was up-regulated by retinoic acid (RA) (Imai et al. 1995). This mouse homolog shares between 84 and- 86% similarity with the human RAI1 protein (Bi et al. 2004; Toulouse et al. 2003). RAI1 functions as a transcription regulator and chromatin binding module, either binding directly to its target or acting in a multi-component complex during development (Bax and Zies 2011; Bi et al. 2004; Burns et al. 2010). RAI1 has higher levels of expression in the brain and the heart (Bi et al.2004; Toulouse et al. 2003). *RAI1* can either be deleted or mutated in patients with SMS, and phenotypes have been found to be more

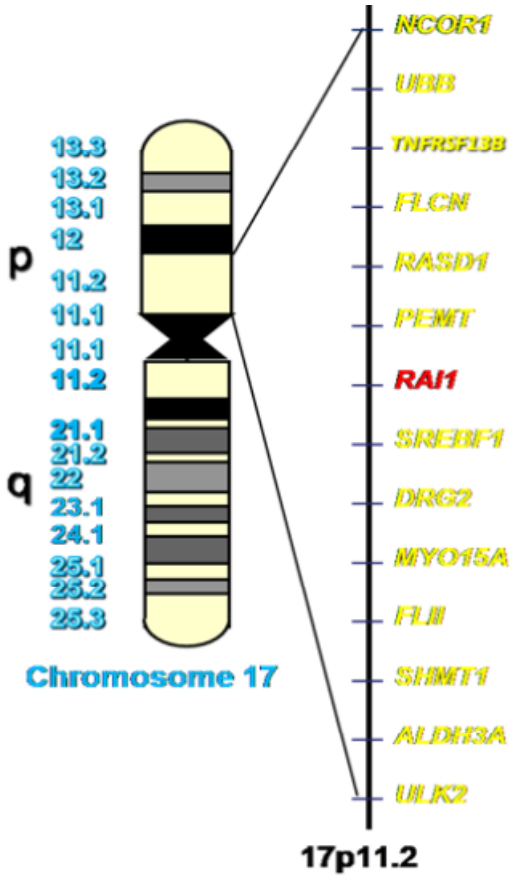

Figure 13. Gene map of Chromosome 17 showing genes in the 17p11.2 region. Included in the region is RAI1, the gene either deleted in Smith – Magenis Syndrome, or duplicated in Potocki-Lupski syndrome.

Source: (Vyas 2009)

severe in deletion patients than those with mutations (Bi et al. 2004; Girirajan 2005; Girirajan 2006; Elsea and Girirajan 2008).

Structure of the *RAI1* gene and RAI1 protein

The human *RAI1* gene consists of 6 exons, of which 4 exons actually code for the RAI1 protein (Exons III – VI) (Figure 14) (Elsea and Girirajan 2008). Exon III makes up more than 95% of the coding sequence, and contains all of the known mutations (Elsea and Girirajan 2008). The RAI1 protein consists of 1906 amino acids and the 7,663 nucleotide mRNA is generated by the six exons in the *RAI1* gene (isoform a) (Figure 14) (Elsea and Girirajan 2008, Toulouse 2003). The RAI1 protein contains a protein homeobox domain (PHD) zinc finger domain at the carboxyl end coded by the end of exon III through exon V (Bi et al. 2004; Toulouse et al. 2003). This PHD finger is conserved in a mouse Rai1 homolog splice variant (GeneBank accession no. AY548172) (Bi et al. 2004). This PHD domain is involved in binding nucleosomes and in the formation of a chromatin remodeling complex and transcriptional regulation (Bienz et al. 2006; Milne et al 2002; Nakamura et al. 2002). Two nuclear localization signals (NLS) are also located in the middle of the protein (Bi et al. 2004; Carmona-Mora 2012). When Neuro-2a cells are transfected with an *RAI1* construct that includes a frameshift mutation coding for a stop codon before the nuclear localization sequences, RAI1 protein localizes in the cytoplasm (Bi et al. 2004). Within the N-terminus of the protein lies a polyglutamine tract, which can vary in size between 10 and 18 repeats in normal individuals (Bi et al. 2004). The size of the repeat is shown to be associated with the age of onset for spinocerebellar ataxia (Hayes et al. 2000). Finally, the RAI1 protein contains two poly-serine tracts, one each in the N and C-termini, similar to the denatorubral-pallidoluysian atrophy (*DRPLA*) and drosophila hairless genes (Carmona-Mora and Walz 2010).

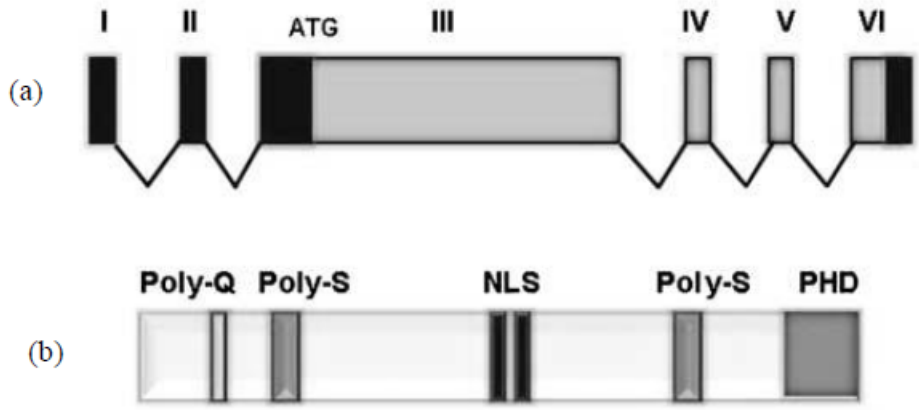

Figure 14. Diagrams of the *RAI1* gene and protein. A, *RAI1* (isoform a) consists of six exons with exons III – VI coding for the RAI1 protein, B, RAI1 protein structure, the protein contains to poly-serine regions in the N-terminus and C-terminus ends, a poly-glutamine region at the N-terminus region, two nuclear localization signals in the C-terminus end, and a PHD zinc finger domain in the C-terminus region of the protein.

Source: (Elsea and Girirajan 2008, Toulouse 2003)

RAI1 is also found to bind the promoter of a key regulator of the circadian rhythm cycle, Circadian Locomotor Output Cycles Kaput (*CLOCK*), a gene involved with the circadian rhythm cycle (Bax and Zies 2011; Williams et al. 2012). The binding site is located within an enhancer region of intron 1 of *CLOCK*, and the enhancer binding region was isolated to 51 bp via the $CLOCK^{Del5}$ construct (Williams et al. 2012).

Zebrafish Model

The zebrafish (*Danio rerio*) is a tropical freshwater fish that is used as a model organism for forward genetic and chemical screenings (Lieschke and Currie 2007). Zebrafish have been used in research as developmental and embryological model since the 1930s (Lieschke and Currie 2007). Zebrafish hold a unique balance between popular model organisms ideal for large scale forward genetics screens as well as random mutation-based reverse genetics. This screening can be achieved in mice as well, but the resource for a large-scale effort with mice requires significant resources, staff, and money. When compared to mice, Zebrafish have a higher fecundity, external fertilization and development, lower costs, and transparent embryos. These advantages allows for unparalleled advantages when studying *in vivo* cell-biological events and development. Many argue that *Caenorhabditis elegans* or *Drosophila melanogaster* has many of the same features; however, the vertebrate relevance of zebrafish makes it a more suitable model to study human congenital disease during development. These characteristics make zebrafish an ideal model organism for studying the neurological and craniofacial development found in Smith – Magenis syndrome patients.

The zebrafish has been used extensively as a model organism for the study of autism spectrum, ID, and craniofacial abnormalities. Kvarnung and colleagues investigated the morphological effects of knocking down the zebrafish homolog (*pigt*) of the

phosphatidylinositol-glycan biosynthesis class T (*PIGT*) gene, known to have homozygous mutations in a novel ID syndrome (2013). Schuurs-Hoeijmakers and colleagues utilized zebrafish to investigate mutations in the phosphofurin acid cluster sorting protein 1 (*PACS1*), a gene implicated in an ID and abnormal craniofacial phenotype, finding that *de novo* mutations in *PACS1* cause a hitherto unknown ID syndrome (2012). Beunders and colleagues investigated the effect of exonic deletions of the autism susceptibility candidate 2 (*AUTS2*) gene in zebrafish and helped establish a hitherto syndromic phenotype (2013).

Aims

- We hypothesize that there is maternal *rai1* expression during zebrafish embryogenesis.
- We hypothesize that a both a haploinsufficiency and complete loss of *rai1* will induce a morphological phenotype in zebrafish, with a complete loss of *rai1* inducing a more severe phenotype; furthermore, we hypothesize that downstream targets such as *bdnf* will be down regulated due to the reduced expression of *rai1*, leading to abnormal neural development.
- We hypothesize that a *rai1* MO will induce a morphological phenotype as it will allow us to investigate if knocking down maternal *rai1* protein.
- We hypothesize that retinoic acid will induce *rai1* expression during all stages of zebrafish embryogenesis, and we will see an increase of *rai1* expression compared to a RA signaling pathway inhibitor (RA) and vehicle (DMSO) treated embryos.

CHAPTER 2: Analysis of Temporal Expression of *rai1* during zebrafish development

Introduction

The zebrafish *rai1* gene

A homolog of the zebrafish *rai1* gene (ENSDART00000106680) was identified and fully annotated in Ensembl Genome Browser. The *rai1* gene maps to chromosome 3 and consists of three exons totaling 5,811 base pairs long, coding for a 1,936 amino acid protein (ENSDARP00000097458) (Figure 15). Furthermore, the full length *rai1*gene shares 27 percent identity with the human *RAI1* gene (Tahir et al. 2014).

Prior Research

Previously, Tadros and Lipshitz found that the zebrafish embryo undergoes a maternal-to- zygotic transition at 3 hours post fertilization (hpf) (2009). Between the hours of 0 and 2 hpf, the embryo relies on only maternal transcript; however, at around 3 hpf, zygotic transcript begins to

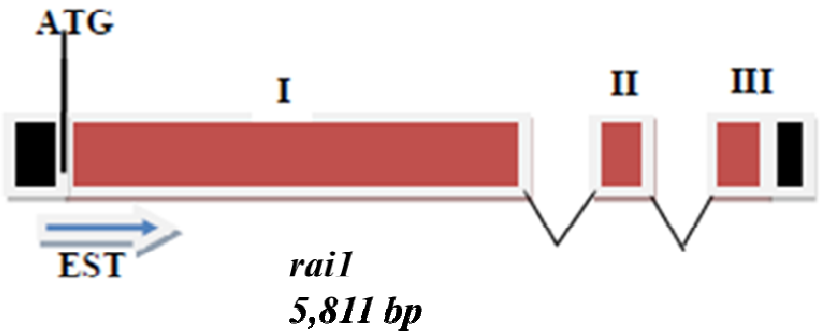

Figure 15. Annotated structure of the zebrafish *rai1* gene. The zebrafish *rai1* mRNA consists of three exons totaling 5,811 bp and codes for a 1,936 amino acid protein.

Source: (Vyas 2009)

play a major role in supporting embryo development with the first wave of zygotic genome activation (ZGA) (Tadros and Lipshitz, 2009). Furthermore, maternal transcript begins to disappear in the embryo due to degradation beginning at around 2 hpf; however, the majority of maternal transcript degradation can occur before, during, or after the first wave of ZGA (Figure 16, Figure 17) (Tadros and Lipshitz, 2009). With this known, Vyas conducted a temporal analysis of *rai1* expression using several time points of early stage zebrafish embryos (2009) (Figure 18). A temporal profile of *rai1* expression is necessary in order to elucidate the active role of *rai1* in zebrafish neurodevelopment. Understanding when *rai1* expression begins during the early stages of development may allow us to understand if maternal *rai1* transcripts play a role in zebrafish embryonic development (Figure 18). If there is maternal *rai1* expression, we will investigate if a haploinsufficient or homozygous mutant zebrafish can survive without maternal *rai1* expression during the earliest stages of zebrafish embryogenesis.

Aims

- We hypothesize that there is maternal *rai1* expression during zebrafish embryogenesis.
    - We will obtain a reproducible temporal expression profile of *rai1* in zebrafish embryogenesis, to determine whether or not maternal *rai1* expression occurs.
        - We will conduct a time point course of end-point PCR using primers for *rai1* and *tcof1*.
        - We will conduct quantitative PCR (qPCR) in order to obtain a quantifiable profile of *rai1* expression in comparison to an endogenously expressed gene during zebrafish embryogenesis.

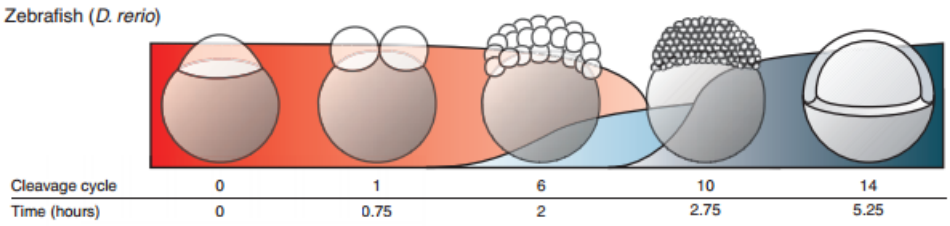

Figure 16. An overview of the maternal-to-zygotic transition in zebrafish. Key developmental stages are shown with the corresponding cleavage cycle and time post fertilization. The red curve represents the degradation of maternal transcripts. The light and dark blue waves represent the minor and major waves of zygotic genome activation, respectively. By 5.25 hours post fertilization, development depends primarily on zygotic transcripts.

Source: (Tadros and Lipshitz 2009)

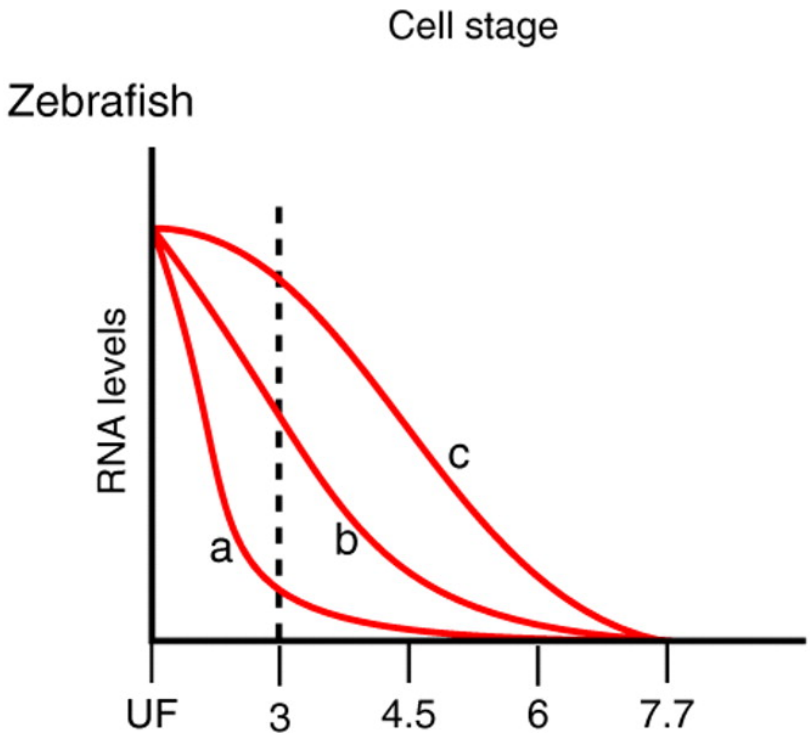

Figure 17. Graph illustrating degradation profiles of maternal transcripts during the maternal-to-zygotic transition. In zebrafish embryos, there are three groups to which transcripts that degrade can be assigned based on whether the majority of their degradation occurs (a) before, (b) during, or (c) after zygotic genome activation (ZGA). The dotted lined denotes the timing of the first major wave of ZGA

Source: (Tadros and Lipshitz 2009).

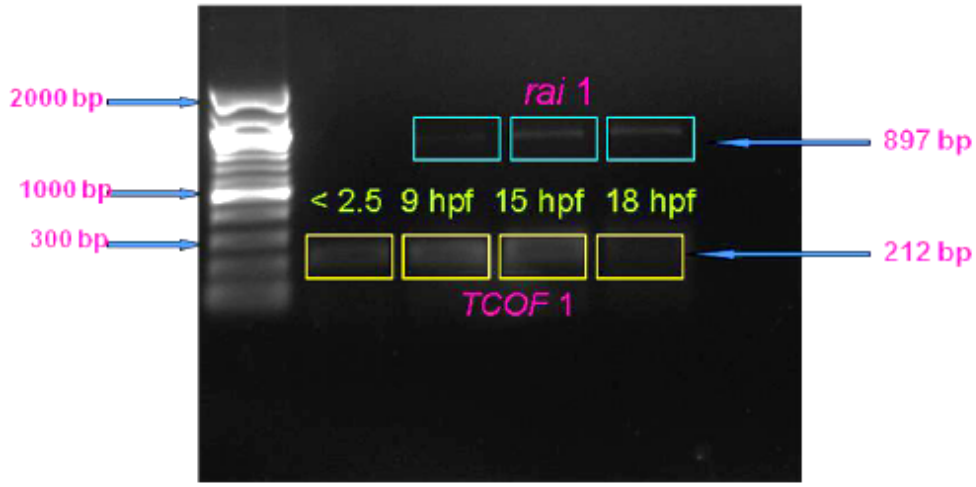

Figure 18. Gel electrophoresis results from RT-PCR of *rai1* for various embryonic time points. Note labeling of the *rai1* and hyperladder sizes, as well as the faint bands present for the *rai1* or *TCOF1*control.

Source: (Vyas 2009)

Materials and Methods

Collect Cultivated Embryos

Embryos were obtained from timed, natural matings, and placed in 10 cm petri dishes with embryo medium. 3 ul of methylene blue was added to each dish to prevent fungal growth. Each petri dish contained approximately 75 embryos, and were placed in incubators set for 28.5º C. The petri dish water was maintained daily by removing empty chorions and deformed embryos.

Time point collection and RNA Extraction

At the seven designated time points (2, 6, 9, 11, 13, 16.5, and 19 hpf), embryos were dechorionated and stored in 1 ml of TRIzol at -80º C until all time points were collected. Each time point had approximately 40 embryos collected. At the completion of the time-course, embryos were homogenized and total RNA was extracted from the TRIzol treated embryos using the protocol supplied by Life Technologies.

Reverse-Transcriptase PCR (RT/PCR)

First strand cDNA synthesis was performed on the extracted RNA from 2, 6, 9, 11, 13, 16.5, and 19 hpf embryos in accordance with the manufacturer's protocol (Stratagene Accuscript) using 1 to 2 µg of total RNA, Accuscript RT, Accuscript RT buffer, oligo-DT (15), 10 mM dNTP mix, RNAsin and DTT.

PCR Amplification

cDNA was PCR amplified with GoTaq polymerase using the following primers that span intron/exon boundaries: JAL754 (CAC CGG CGT CCG GAT GCC AAG GTG AAG G) starting in exon two heading 5' to 3' (Figure 19), and primer JAL766

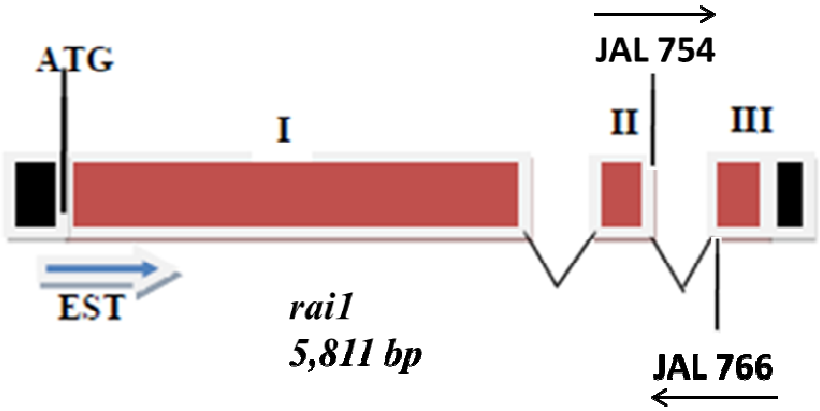

Figure 19. Diagram illustrating PCR amplification of cDNA obtained from RT PCR. Primers JAL754 and JAL766 span intron/exon boundaries so amplification will amplify any reverse-transcribed cDNA from the RNA present in the embryos.

Source: (Vyas 2009)

(CAC ACT TAC CTT GTG TTT GGA CAC) starting in exon three heading 3' to 5'. Primers were diluted to 10 picomoles/microliter, with 1 µl of forward and reverse primers used, 2µl of H_20, 1 µl of cDNA, and 5 µl of GoTaq master mix (Promega) used in each PCR reaction. PCR samples were run for each time point with an RT neg-control and positive control using 19 hpf cDNA with *nolc1l* primers Z3818911F (GCG ATC TCT ACC AAC ATG TG) and Z3818911R (CTT GGC TGA TGG GCC ATT GA). The PCR was run with a 60º C annealing temperature for 35 cycles with an extension time of 30 seconds per cycle.

PCR products were electrophoresed in 1.2% agarose gels containing GelRed for resolution of DNA. 5 µl of each PCR product was loaded into each well with Hyperladder I in the first and last lane as DNA markers. The gel was run for 45 minutes at 100 V.

Quantitative PCR (qPCR)

RNA that was extracted from the various time point embryos was used for qPCR with the primers JAL826 (F, ATTACAGATGGAGGCCGAGG) and JAL827 (R, TTCTTCTTCAAACGTGCAGC), which were created with Primer3 (http://bioinfo.ut.ee/primer3/). Appropriate dilutions of the RNA were made to ensure equal amounts were present at each time point. *rai1* expression was compared to that of **β**-actin; furthermore, three negative control wells were included for both *rai1* and **β**-actin, where no cDNA was added to the master mix containing Sybr Green (Quanta), RNAse free water, and primers.

Results

rai1 expression

Due to the irreproducibility of the Vyas' results using the same primers (Figure 20), the temporal analysis experiment was repeated. When we looked at *rai1* expression using RT-PCR, the expected *rai1* band (A, ~192 bp) expression is found in all time points (Figure 21). There are several lanes with genomic amplification (B, ~892 bp) (Figure 21). The primers JAL 754 and JAL 766 amplify a region beginning at the end of exon two to the beginning of exon three, spanning intron/exon boundaries. In addition to cDNA, primers JAL 754 and 766 amplified genomic DNA, which included intron two, leading to the ~892 bp band. Primer dimers are found below the *rai1* bands in all time points (except 13 hpf) as well as for the negative control. The *nolc1l* positive control band (~212 bp) can be found just above the 200 bp marker, and was used to as a positive control to show there was proper amplification with the same RNA. .

Quantitative analysis

qPCR was performed and showed that there was a significant drop off in *rai1* expression during the course of embryogenesis (Figure 22). There is a 0.2 fold decrease in *rai1* expression between 2 and 6 hpf when compared to actin. The largest reduction in *rai1* expression is between 6 and 9 hpf , where expression drops to nearly zero. Further into the qPCR data, we see limited upregulation of *rai1* as we move through the 11 and 13 hpf time points. Finally, we see a downregulation in the subsequent time point (16 hpf) and second upregulation of *rai1* in the final time point (19 hpf).

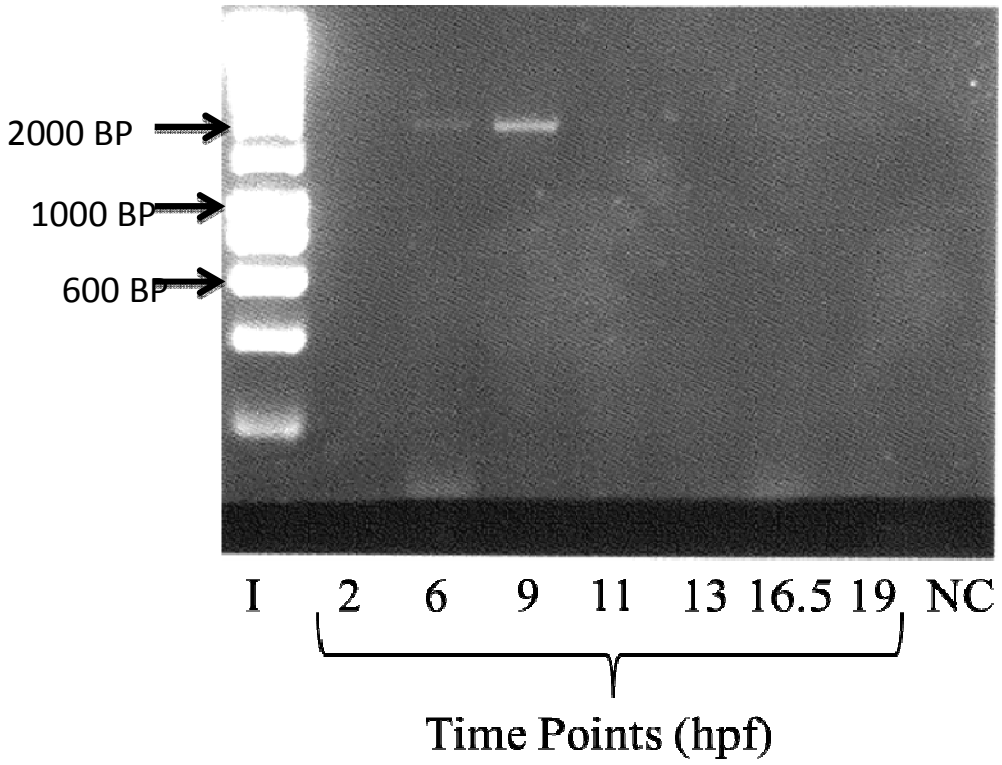

Figure 20. Gel electrophoresis of repeated temporal expression experiment conducted by Vyas. PCR products were made using new SHE646 and SHE650 primers, with the same PCR cycling parameters that Vyas utilized. The samples were run on a 1.2% gel for 45 minutes. Lane one is shown with a DNA marker (Bioline Hyperladder I). Lanes 2 through 8 are time points studied for *rai1* expression. Lane 9 is a negative control (NC) for the PCR amplification. As shown, there is no consistent amplification of the *rai1* transcript by the primers SHE646 and SHE650 that was shown by Vyas previously. This gel is the best of several attempts with new SHE646 and 650 primers to reproduce the results.

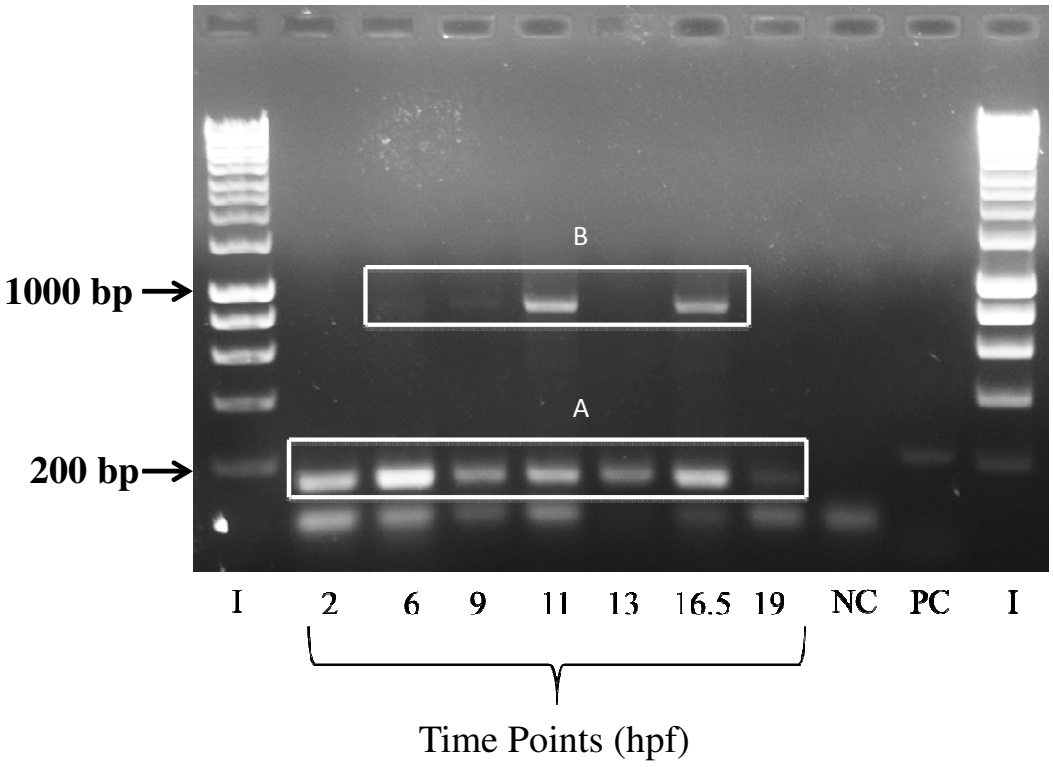

Figure 21. PCR of cDNA showing *rai1* expression at various time points during zebrafish embryogenesis. Gel electrophoresis results from the *rai1* PCR using cDNA generated from RT/PCR from 2, 6, 9, 11, 13, 16.5, and 19 hpf RNA extractions shown in Figure 19. Lanes 1 and 11 contain hyperladder I as a size marker. Lanes 2 through 8 are PCR samples from 2, 6, 9, 11, 13, 16.5, and 19 hpf. Lane 9 is a negative control (NC) with lane 10 as a positive control (PC) for the PCR. The presence of two sets of bands below 200 base pairs shows the *rai1* amplification (A, approximately 192 bp), with the smallest band representing primer dimers that were formed from JAL754 and JAL766 primers. The 6, 9, 11 and 16.5 hpf PCR runs show genomic amplification, with bands approximately 900 base pairs in size (B). Just above the 200 base pair marker in lane 10 is the *nolc1l* positive control, which is approximately 212 base pairs in size.

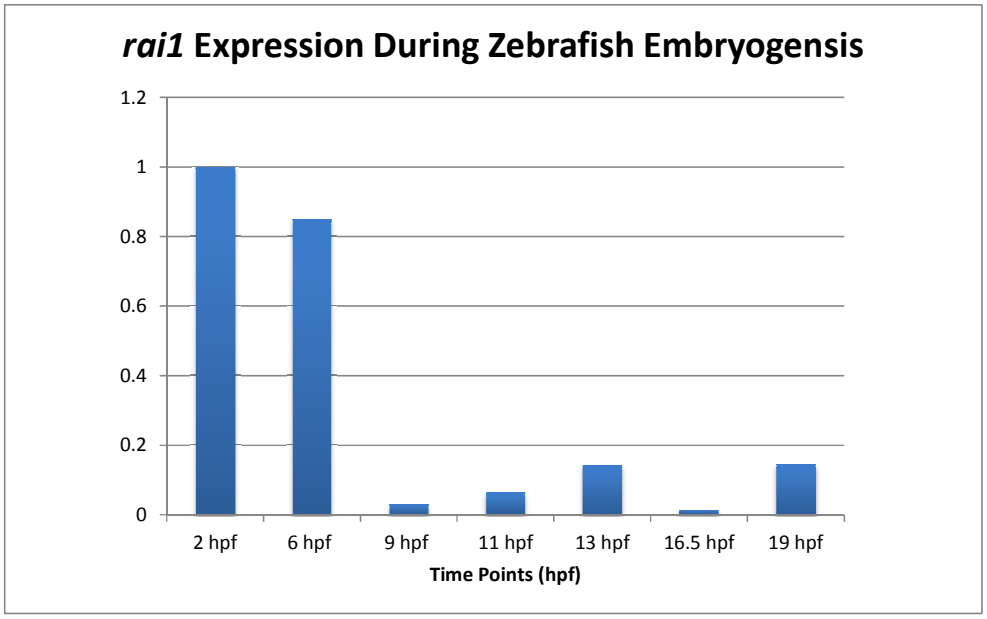

Figure 22. *rai1* expression levels drop significantly after 6 hpf. The expression levels of *rai1* in zebrafish embryos during embryogenesis slightly reduce to approximately 0.8 fold between 2 and 6 hpf. The largest reduction occurs between 6 and 9 hpf, where *rai1* expression reduces to nearly 0. *rai1* expression increases from 9 to 13 hpf, dropping again to its lowest expression value at 16.5 hpf. Finally, *rai1* expression increases slightly between 16.5 and 19 hpf.

Discussion

Maternal *rai1* expression is present during zebrafish embryogenesis.

Based on the end-point PCR experiment, there was visible expression at 2 and 6 hpf, when zygotic expression begins to make up the majority of mRNA expressed in the embryo (Tadros and Lipshitz 2009). Furthermore, there is maternal *rai1* expression in the embryo, which can be seen at 2 hpf. The presence of genomic amplification can be explained due to genomic contamination. The temporal expression data provide evidence supporting the presence of maternal *rai1* expression during the earliest embryonic development in zebra fish; however, the findings do not explain what role the maternal *rai1* expression has on other genes and whether or not it is vital for development. Haploinsufficiency of maternal *rai1* may lead to behavioral phenotypes due to the fact that maternal *rai1* may regulate expression of several downstream targets including *clock* during the first 5 hours of fertilization (Burns et al. 2010, Bax and Zies 2011; Tadros and Lipshitz 2009).

The qPCR data presents interesting findings, which can be supported by the findings of Tadros and Lipshitz (Figure 16, 17) (2009). The data from the qPCR shows that there is a *rai1* expression at 2 hpf, which at that point would be maternal transcript (Figure 16) (Tadros and Lipshitz 2009). Tadros and Lipshitz write that there are two significant waves of zygotic gene expression in the embryo, at around 1.5 and 3 hpf, with development depending primarily on zygotic transcripts (Figure 16, 17) (2009). Furthermore, we also see that maternal transcript (red curve) is very high from fertilization through about 2 hpf, after which the levels of maternal transcript begin to decrease (Figure 16) (Tadros and Lipshitz, 2009). The qPCR data show that *rai1* expression at 6 hpf is at about 0.8 relative to the 2 hpf expression values. This reduced *rai1* expression may coincide with group c transcripts found in Figure 17 (Tadros and Lipshitz 2009).

If *rai1* were in fact a group c transcript, then the majority of maternal transcript degradation would occur after the ZGA and thus we would still see *rai1* expression (from maternal transcript) present at 6 hpf (Tadros and Lipshitz 2009). The qPCR expression graph shows *rai1* expression to be almost zero by 9 hpf. This may be due to the fact that nearly all of the gene expression in the embryo is carried out by zygotic transcript, with *rai1* activation being limited at this point. Reviewing the 11 hpf – 19 hpf time points show two potential upregulation times of *rai1* during embryogenesis, where *rai1* may be needed for development. Finally, error bars are not present on the graph due to only running the qPCR one time and additional qPCRs are necessary to validate the findings.

The end-point PCR and qPCR results are a bit contradictory to one another, as the first shows a more consistent expression profile amongst all time points, while the qPCR shows a drop off in expression. We believe the quantitative results are more accurate because the qPCR is measuring *rai1* expression relative to an endogenous gene present in the embryos, *actin.* qPCR measures the DNA in real time as the reaction is occurring; while end-point PCR is merely looking for the presence of expression and not a quantifiable amount of expression or said expression relative to an endogenous gene.

CHAPTER 3: Loss of function of *rai1* in zebrafish embryos

Introduction

Extensive research has been conducted to elucidate the morphological effects of the haploinsufficiency or full loss of *RAI1* and its various homologues in various organisms. First reported in 1986 by Smith and Magenis, patients with SMS present characteristics including intellectual disabilities, ocular abnormalities such as retinal detachment (Finucane and Jaeger 1997), otolaryngological abnormalities including mild hearing impairment and throat polyps (Greenberg et al. 1996), skeletal abnormalities including scoliosis (Tsirrikos et al. 2010) and brachydactyly (Elsea and Girirajan 2008), as well as craniofacial abnormalities such as frontal blossing and a tented upper lip (Allanson et al. 1999; Elsea and Williams 2011; Tomona et al. 2006). In the mouse, a haploinsufficiency of *Rai1* leads to learning impairment, craniofacial abnormalities including shorter snouts and concaved nasal bones, system manifestations including obesity (Burns et al. 2009; Bi et al. 2005). In homozygous mutant *Rai1* mice, the same craniofacial defects were observed as well as axial skeleton defects including hypoplastic hyoid bones (Bi et al. 2005). More recently in *Xenopus*, Tahir and colleagues found that a reduction of

Rai1leads to increased forebrain apoptosis, decreased *bdnf* expression, as well as defects in brain morphology and axon patterns (Tahir et al. 2014).Using a *Rai1* morpholino oligonucleotide (MO), the team also found that reduced amounts of Rai1causes abnormal development throughout the body, with compounding craniofacial abnormalities of altered shapes and sizes of *Xenopus* embryo faces (Tahir et al. 2014). Based on these findings, it would be logical to investigate the potential morphological phenotypes with down regulation of *rai1* in zebrafish, a true genetic aquatic model organism.

The lab possesses an *rai1* MO generated against the ATG of the zebrafish *rai1* gene and was injected in 1 cell stage Zirc AB embryos to observe whether knock down causes a morphological phenotype.

A *rai1* loss-of-function mutation was discovered in a frozen sperm sample in November 2012 by the Moens Zebrafish TILLING (Targeted Induced Local Lesions in Genomes) project (http://webapps.fhcrc.org/science/tilling/index.php). TILLING, a reverse-genetics method, utilizes a chemical mutagen such as ethylnitrosourea (ENU) to induce mutations in male zebrafish, and the males are then outcrossed to create an F_1 population. Males from the F_1 population are then used to create DNA and sperm libraries, with these libraries being screened for the target loci by TILLING. TILLING uses PCR to amplify the exons of genes of interests, and subsequently using various heteroduplex or direct sequencing techniques, identify mutations in the gene of interest. Once a mutation of interest (*fh370*) was identified in one of the males, sperm samples were used to generate offspring via in vitro fertilization (IVF). The fertilized eggs were recovered and offspring were grown to adult maturity. The mutation was confirmed via sequencing by the Fred Hutchinson Research group.

There are seven important stages in zebrafish embryogenesis, these include: zygote, cleavage, blastula, gastrula, segmentation, pharyngula, and hatching stages (Kimmel et al. 2005). The zygotic stage, a single cell stage, occurs between 0 – 45 minutes post-fertilization. During the zygotic stage, the cytoplasm migrates toward the animal pole to form the blastodisc. In the cleavage stage, there is synchrony of cell division to the 64 cell stage where a 3 tier blastodisc forms between 45 minutes and 2 hours post-fertilization (hpf). During the blastula stage, there is synchrony of cell division through 1000 cells, where an 11 tier blastodisc forms by 3 hpf. The marginal blastomeres join the yolk cells to form the yolk syncytial layer (YSL), and the YSL begins non-synchronous cell division in multiple layers. As the YSL continues to multiply, the blastodisc flattens and forms a perfect sphere between the blastodisc and yolk. The yolk cells then bulge toward the animal pole while prominent and rapid changes continue between the blastodisc and yolk cells, thus beginning epiboly. During epiboly, the blastoderm thins and spreads to completely cover the yolk cell over six hours, with gastrulation beginning about 1 hour into epiboly (Warga and Kimmel 1990). At around 4 hours and 40 minutes post-fertilization, 30% of the epiboly is completed (Kimmel et al. 2005). During the gastrula stage at around 75% epiboly, the eight hour blastoderm begins to thicken on the dorsal side; by nine hours and 90% epiboly, postmitotic cells appear and form the notochord, axial-derived muscles, and specific neurons in the hind brain. At ten hpf and the end of gastrulation (bud stage), the embryo develops completes epiboly and has a prominent tail bud and early polster, the hatching gland underlying the forebrain during early segmentation (Kimmel et al. 1995). The segmentation stage occurs between 10.33 and 24 hpf, and in this stage the embryo begins to develop primordial regions such as the optic primordium (four somite) and the midbrain-hindbrain boundary (MHB) (26 somite) has formed. At 24 hpf, we also see the beginning of

melanogenesis; the heart begins to beat, and the initiation of primary body organ formation such as the brain, retina, and inner ear. By 48 hpf, the otic vesicle develops, the yolk size reduces as the size of the head increases, the first hair cells begin to differentiate, and fin buds develop into a long pectoral fin. At 72 hpf, the majority of organs have finished morphogenesis including the development of the gills, jaw and pectoral fins. The swim bladder can be observed between the yolk and notochord.

Aims

- We hypothesize that a *rai1* MO will induce a morphological phenotype as it will knockdown maternal *rai1* transcript.
    - *rai1* MO will be injected, alongside a control, into Zirc AB embryos and observe for a morphological phenotype.
- We hypothesize that a both a haploinsufficiency and complete loss of *rai1* will induce a morphological phenotype in zebrafish, with a complete loss of *rai1* inducing a more severe phenotype.
    - We will intercross *rai1 +/rh370* fish and observe *rai1 +/rh370* and *rai1 rh370/rh370* embryos for a morphological phenotype.
- We hypothesize that downstream targets such as *bdnf* will be down regulated due to the reduced expression of *rai1* in both *rai1 +/rh370* and *rai1 rh370/rh370* embryos, leading to abnormal neural development.
    - Conduct ISH on *rai1 +/rh370* intercross larvae at 48 and 72 hpf to observe for normal *bdnf* expression.
    - Conduct whole mount immunostaining on *rai1 +/rh370* x neuroD:GFP larvae to observe neural development.

Materials and Methods

Morpholino Injections

Wild-type embryos were obtained from adults of the AB strain (obtained from the Zebrafish International Resource Center [ZIRC], Eugene, OR) and three cohorts were established at the 1 cell stage. One cohort contained wild type embryos not injected with a morpholino, another cohort was injected with 10 ng of rai1 morpholino (CACTCCGCTCTCTGAAGGACTGCAT), obtained from Gene-Tools LLC, Summerton, OR) only, and the last cohort was injected with both 10 ng rai1 morpholino, as well as 2.5 ng of tp53 morpholino to be used as a control.

Genotyping

The TILLING-identified mutation, called *fh370* (courtesy of Fred Hutchinson Cancer Research Group), is a single nucleotide change at position 722 changing a thymine to an adenine. This single nucleotide changes the amino acid at codon 241 from a thymine to a stop. The sperm sample from the identified male was used to fertilize zebrafish eggs via IVF, the embryos were grown up in Seattle, and the lab received 4 identified heterozygous *rai1 +/fh370* mutant adults (1 male and 3 female) in April 2013. The mutation sequence was confirmed through sequencing a homozygous *rai1* -/- male from the F1 progeny.

As *rai1 +/fh370* offspring reached adult maturity, fin clips were taken and DNA was extracted. The embryos were genotyped using primers JAL 771(5'-CTTCTTCACCTTCATCGGCTTA) and JAL 772 (5'–GCTGGGTCTGATTGTAGTGC) designed with dCAPS (Neff et al. 1998). These primers created a mismatch in the PCR amplification, causing a change in one of the bases in the PCR amplified sequence (Figure 24) (Neff et al. 1998). The wild type sequence is CTAT, while the mutant sequence is CTAA (Figure

24). dCAPs introduces a nucleotide change from cytosine to thymine in both the wild type and mutant amplicons (Figure 23). This creates the sequence TTAA within the mutant amplicon, recognized by the restriction enzyme MseI. Digestion of the PCR product with MseI creates a 240 bp band if the mutation is present, and a 262 bp band if the mutation is not present, and (Figure 24). The digested samples were run on a 3% agarose gel with the 100 bp ladder for 1 hour and imaged with an AlphaImager gel camera and accompanying AlphaImager software.

Heterozygous Crosses and Embryo Cultivation

Embryos were harvested and collected as described in Chapter 2. Zirc AB adults were crossed for the morpholino injections, while *rai1* +/*fh370* adults were used for intercross mating.

***In Situ* Hybridization**

Once the embryos were dechorionated, the embryos were fixed at the desired stage in a 1.5 ml Eppendorf tube with 4% Paraformaldehyde (PFA) in 1X phosphate buffered saline (PBS) overnight at room temperature on a 3D rocker (Benchmark Research Products). The next day, the embryos were rinsed out of the fix in three washes of 1X PBT (PBS + 0.05% Tween 20) and dehydrated in 100% methanol (MeOH) for at least 30 minutes to decrease the background. After dehydration, the embryos went through a MeOH/PBT series of one wash of 66% MeOH/33% 1X PBT, one wash with 33% MeOH/66% 1X PBT, and four washes of 100% 1X PBT. Each wash required 1 ml of wash liquid and 10 minutes on the 3D rocker. Following the MeOH/PBT series, embryos past 24 hpf were treated with 1 µg/ml of proteinase K (PK) in 1X PBT for every hour of embryo age (i.e. 27 minutes in PK treatment for 27 hpf embryos). Following PK treatment, PK solution was removed and embryos were post-fixed with 10% formalin for 20 minutes followed

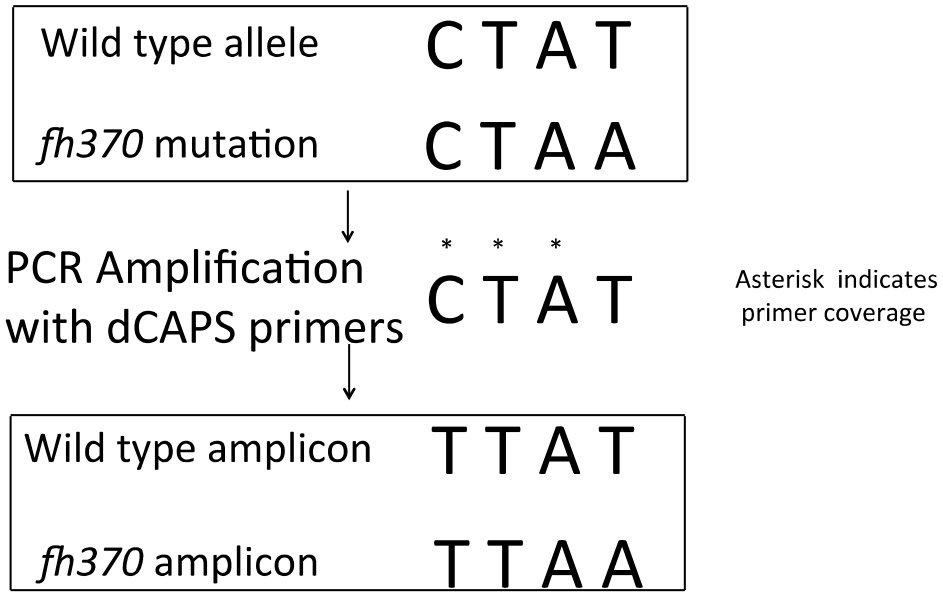

Figure 23. Overview of the wild type and *fh370* alleles undergoing PCR with dCAPS primers. DNA extracted from the +/*fh370* heterozygous zebrafish fin clips contained a wild type allele and an allele with the *fh370* mutation. The DNA is amplified via PCR with dCAPS primers, causing a mismatch in the cytosine base pair, leading to a base pair change in the amplicon. The sequence TTAA is recognized by the restriction enzyme MseI.

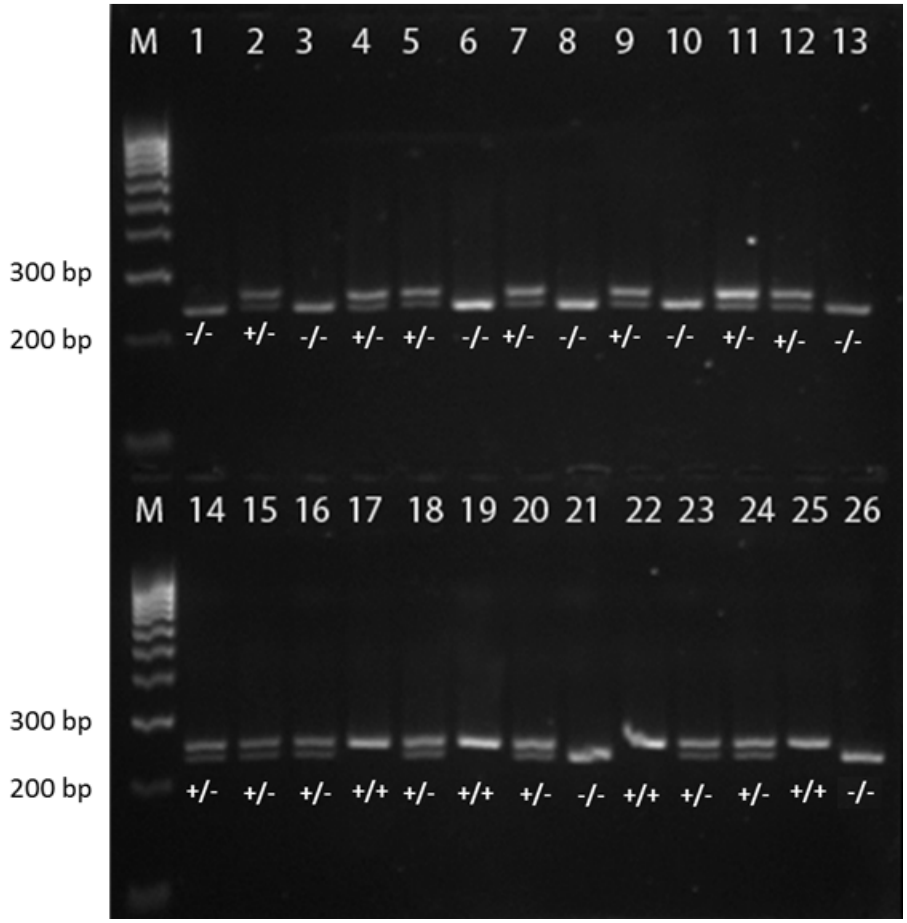

Figure 24. Agarose gel showing genotyping results for four *rai1 +/rh370* intercross embryos. Lanes 1-15 are progeny of a *rai1* -/- female and *rai1* +/- male, shown with 100 bp ladders for DNA markers (M). Lanes 16-26 are progeny of a *rai1* +/- male and female. The +/- genotype is shown by the separation of bands, caused by the identification of the TTAA site by the restriction enzyme *MseI* in mutant alleles, cutting off part of the amplicon and creating a smaller band (lanes 2, 4, 5, 7, 9, 11, 12, 14, 15, 16, 18, 20, 23, 24). The single smallest band designates the -/- mutant genotype (lanes 1, 3, 6, 8, 10, 13, and 26), while the single larger band designates the +/+ genotype (lanes 17, 19, 22, 25).

Formatted: Line spacing: Multiple 1.15 li

by two 1X PBT washes. The embryos were then prehybridized with 500 µl of 1X Hyb mix + tRNA and heparin (Hyb+) for at least an hour in a 65ºC water bath. While the embryos were prehybridizing, the probe stock was diluted to 1:200 in Hyb+ and preheated in a 65ºC water bath. After at least an hour, the prehybridization solution was removed from the embryos and the prewarmed diluted probe was added (usually 500 µl for 10 – 50 embryos) and the embryos were left in a 65ºC water bath O/N. Following overnight hybridization at 65ºC, 1X Hyb mix –tRNA and heparin (Hyb-) was preheated to 65ºC. The diluted probe was then removed and saved for later use, and 500 µl of 1X Hyb- was added to the embryos as a quick wash. Subsequent 500 µl washes of 66%Hyb-/33% 2X sodium chloride sodium citrate buffer (SSC), 33%Hyb-/66% 2XSSC, and 100% 2XSSC were all one time each for 10 minutes in a 65ºC water bath. The next 500 µl 0.2XSSC wash was done twice for 20 minutes in a 65ºC water bath. The next three 1000 µl washes, 66% 0.2XSSC/33% 1X PBT, 33% 0.2XSSC/66% 1X PBT, and 1X PBT, are completed for 5 minutes on the 3D shaker at room temperature. While incubating, block solution was made, with 1 ml of block is needed per sample. The block solution consisted of 880 µl of 1X PBT, 100 µl of bovine serum albumin (BSA), 20 µl of goat serum (GS) per 1 ml of block solution. The last 1X PBT wash was removed and 500 µl of block solution is added and the embryos incubate in the solution on the 3D rocker for at least an hour at room temperature. During the one hour incubation, a 1:10 dilution of anti-Digoxigenin was made using block solution. After adding the antibody to the block solution, a 1:10,000 antibody dilution, the block solution without antibody was replaced and the new block solution with antibody was added to the embryos and the embryos were incubated overnight on the tube's side at 4ºC. The next day, a quick wash was performed with 1 ml of 1X PBT followed by five washes using 1 ml of 1X PBT for 15 minutes each wash at room temperature on the 3D rocker. Following the 1X PBT washes,

three washes 500 µl with 1X coloration buffer + 0.1% Tween-20 were performed for five minutes each at room temperature on the 3D rocker. For the coloration reaction, 4.5 µl and 3.5 µl of nitro blue tetrazolium chloride (NBT) [225 µg/ ml] and 5-bromo-4chloro-3'-indolylphosphate p-toluidine salt (BCIP) [175 µg/ ml] respectively was added to each ml of 1X coloration buffer + 0.5% Tween-20, and this was added to each Eppendorf tube of embryos. The tubes were developed in the dark at room temperature, with additional incubation overnight at 4% if necessary. Following the coloration reaction, embryos were quick washed in 1X PBT and then dehydrated in MeOH for 30 minutes to clear out background. The embryos were rehydrated via the MeOH/PBT series and then equilibrated in 1X PBT + 50% glycerol for imaging.

Whole mount immunostaining

rai1 +/*fh*370 adults were mated with neuroD:GFP+ (http://zfin.org/action/fish/fish-detail/ZDB-GENO-080701-3,ZDB-GENOX-080709-22,ZDB-GENOX-120507-2) adults. *rai1* +/*fh370* x neuroD:GFP+ intercross larvae were dechorionated and fixed at 72 hpf in 4% PFA with 1X PBS at 4ºC overnight. The next day, the PFA was aspirated and the larvae were rinsed in 1X PBTx (1X PBS + 0.1% Triton X-100). Following the wash, 1 ml of ice cold acetone was added and the larvae were placed in -20ºC for 7 minutes. After 7 minutes, the acetone was aspirated and the larvae were washed four times with PBTx for 5 minutes each wash. The larvae were then blocked with blocking solution for at least 1 hour on the rocker at RT. After at least 1 hour, the blocking solution was aspirated and replaced with primary antibodies of a rabbit monoclonal antibody against GFP (Life Technologies) and a mouse zn8 antibody, both were diluted 1:1000 in 1 ml blocking solution (1X PBS, 0.2% Triton X-100, 2 mg/ ml BSA, 2% GS, 1% DMSO). The larvae were then placed on a rocker at 4ºC O/N. The next day, the larvae were quick rinsed with 1 ml 1X PBTx, followed by 3 washes for 1 hour each on a shaker at room

temperature. After the three washes, the secondary antibodies of goat anti-rabbit Alexa488 for the GFP primary antibody and anti-mouse Alexa568 for the mouse zn8 primary antibody were added. These larvae were incubated with the secondary antibodies in blocking solution in 4ºC O/N. The next day, the larvae were quick rinsed with 1 ml PBTx and washed 5 times with 1 ml PBTx for 15 minutes each wash, with the larvae tube wrapped in foil. Finally the larvae were equilibrated in 1X PBS/50% glycerol.

Imaging

Images of the embryos were taken with the Olympus DP70 camera and the Olympus SZX12 microscope, using the DP controller computer software.

Results

MO injection study

rai1 MO injections did not induce short term, lethal, morphological phenotypes in the Zirc AB embryos (Figures 25, 26). Approximately 50% of MO injected embryos (not pictured) exhibited a curved body phenotype; however, embryo bodies straightened after 24 hours. Furthermore, 10 mg *MO* embryos showed necrosis throughout the forebrain at 24 hpf (Figure 25, orange arrow), which gradually reduced after 24 hours (Figure 26, orange arrow).Embryos survived after injection, but were not kept in the nursery as they were euthanized at 7 dpf.

***fh370* intercross study**

The four adult *rai1 +/fh370* zebrafish received from the Fred Hutchinson Cancer Research Group were used for population building and subsequent study of morphological phenotypes in their offspring. As +/*fh370* intercross offspring reached maturity, they were

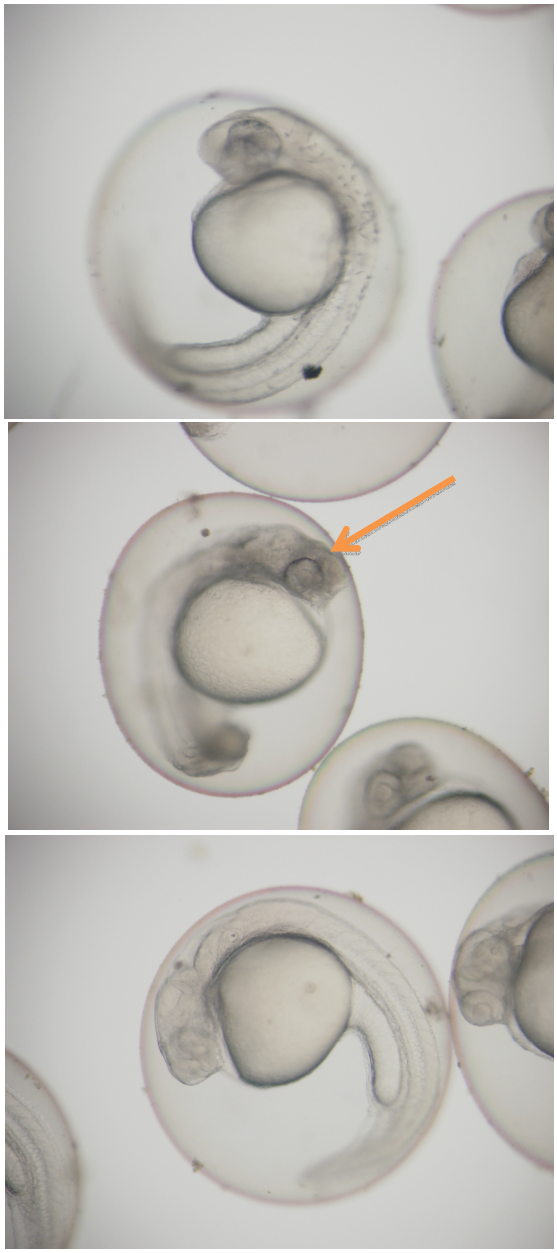

Figure 25. Images showing phenotypes of 24 hpf uninjected and MO injected embryos. Top, uninjected Zirc AB embryos, Middle, 10 mg *rai1* MO injected and, Bottom, 10 mg *rai1* + 2.5 mg tp53 MO injected embryos. Necrosis (arrow) can be seen in the 10 mg *rai1* MO injected embryos in the forebrain of the embryo.

Figure 26. Images showing phenotypes of 48 hpf uninjected and MO injected embryos. Top, uninjected Zirc AB embryos show similar phenotypes as, Middle, 10 mg *rai1* MO injected and, Bottom, 10 mg *rai1* + 2.5 mg tp53 MO injected embryos. Necrosis (arrow) can be seen in the 10 mg *rai1* MO injected embryos in the forebrain of the embryo.

genotyped and a *rai1 +/fh370* population was established. Homozygous mutant *fh370/fh370* male and female zebrafish have been identified and used to reproduce, generating cohorts of fh370/fh370 fish. The mutant allele has been amplified from a male *fh370/fh370* fin clip and inserted into a vector. The vector was sequenced, generating an electropherogram (Figure 27B), and used to confirm the *fh370* mutation was present (Figure 27A).

There was no morphological phenotype present at any developmental stage of the *rai1 +/fh370* intercross embryos, regardless of genotype (Figures 28, 29, 30, & 31). In a clutch from one mating of *rai1 +/fh370* fish (not pictured), we observed a curved shape phenotype and abnormal behavior characterized by swimming in circles for 25% of the embryos but was not seen in any other clutches. Subsequent genotyping (Figure 32) of the embryos showed that this phenotype was not linked with *rai1* mutations because two of the four zebrafish with the curved phenotype were genotyped as *rai1* +/+. Subsequent clutches of embryos did not show this same curved phenotype again.

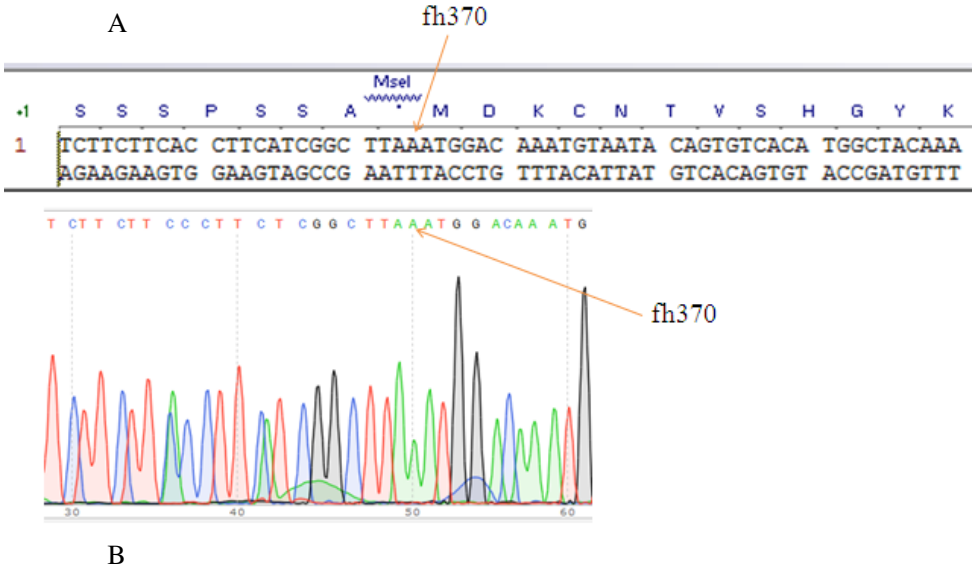

Figure 27. Comparison of mutant allele fh370 sequence to electropherogram confirming the *fh370* mutation. A side-by-side comparison of the sequence (A) and electropherogram (B) confirms the presence of the fh370 mutation a genotyped male *fh370/fh370*.

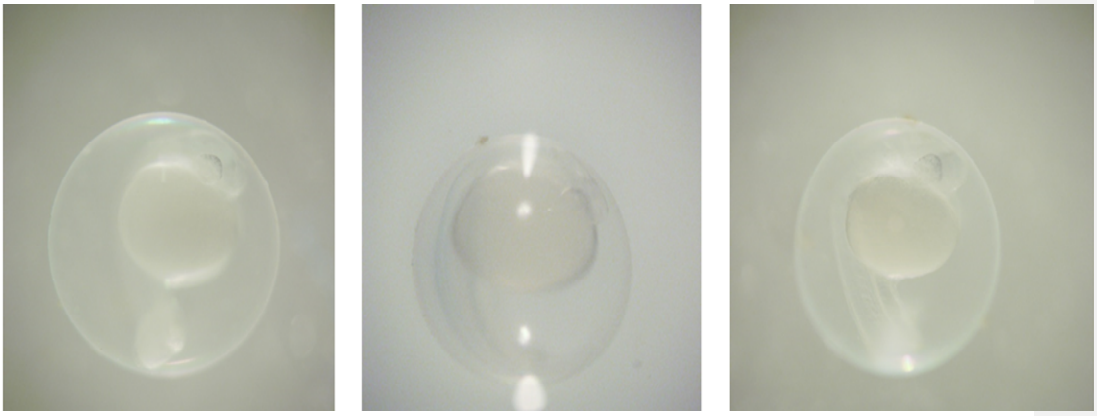

Figure 28. Images of 24 hpf embryos presenting similar phenotypes among all *rai1* genotypes. A, wild type embryos taken at 24 hpf exhibit a similar phenotype compared to both *rai1 +/fh370,* B, and *rai1 fh370/fh370* intercross embryos taken at 24 hpf.

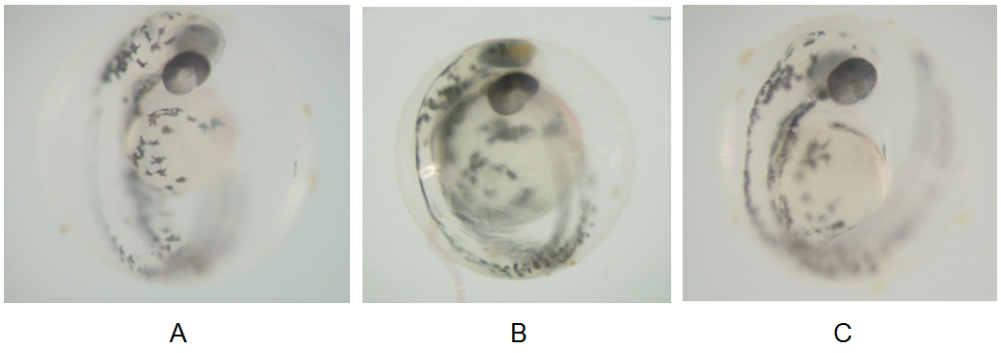

Figure 29. Images of 48 hpf embryos presenting similar phenotypes among all *rai1* genotypes. A, wild type embryos taken at 24 hpf exhibit a similar phenotype compared to both *rai1 +/fh370,* B, and *rai1 fh370/fh370* , C, embryos taken at 48 hpf.

Formatted: Left

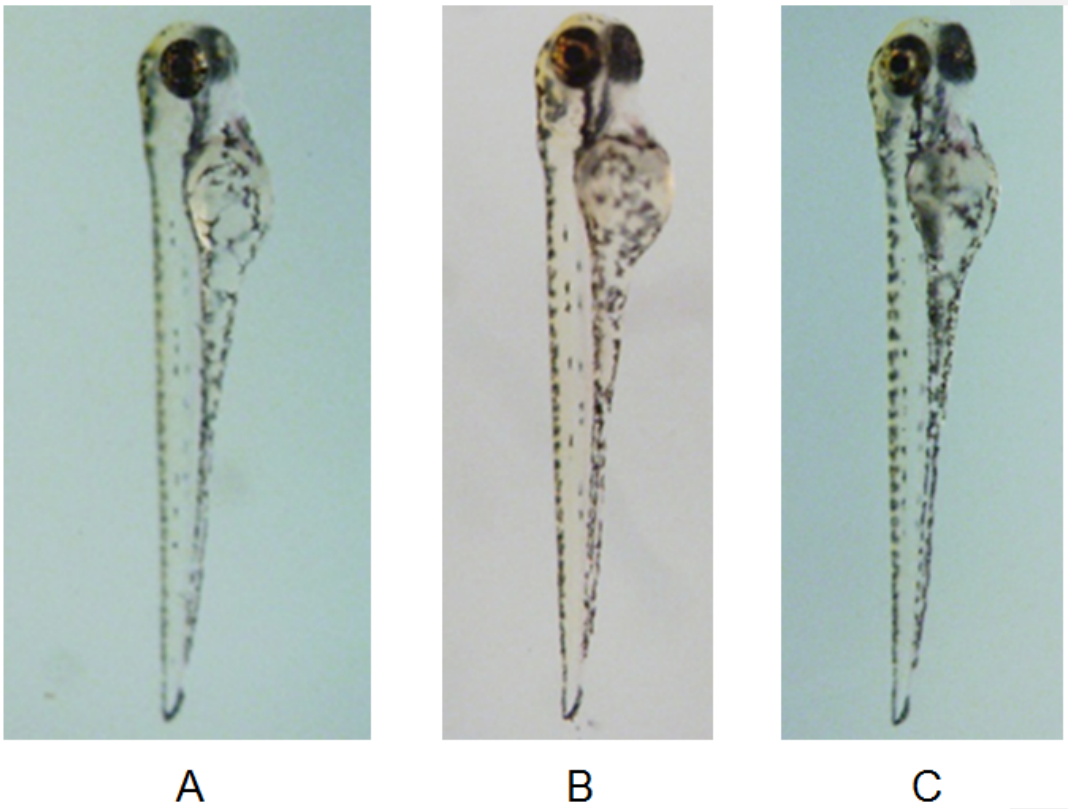

Figure 30. Images of 72 hpf embryos presenting similar phenotypes among all *rai1* genotypes. A, wild type embryos taken at 24 hpf exhibit a similar phenotype compared to both *rai1 +/fh370,* B, and *rai1 fh370/fh370*, C, embryos taken at 72 hpf.

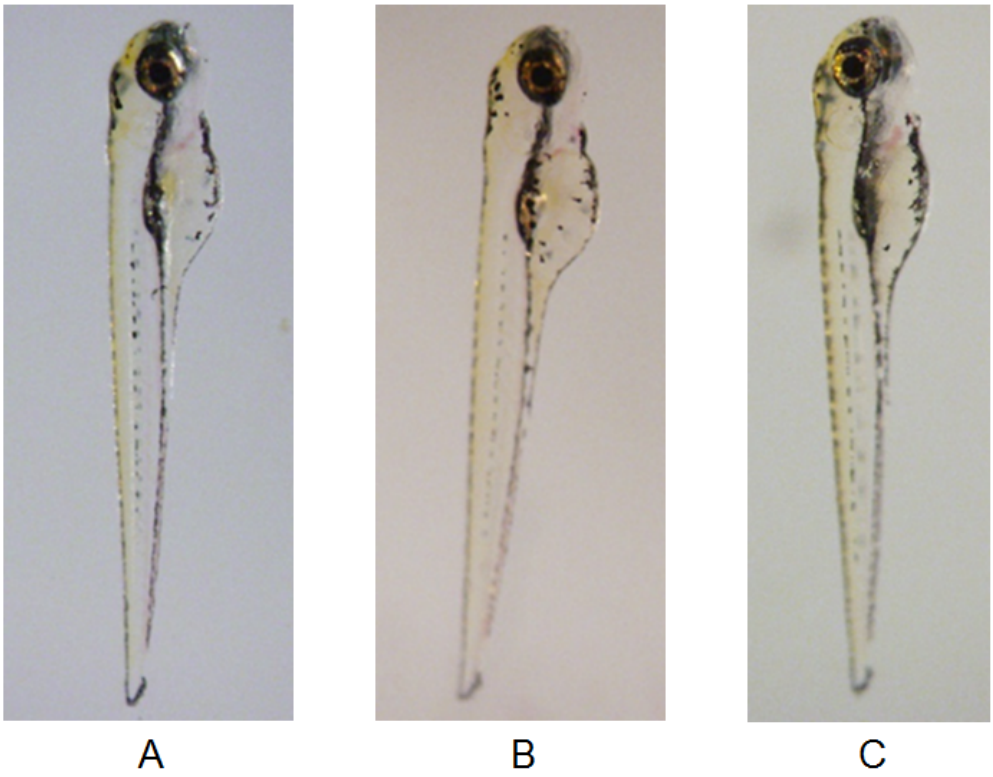

Figure 31. Images of 96 hpf embryos presenting similar phenotypes among all *rai1* genotypes. A, wild type embryos taken at 24 hpf exhibit a similar phenotype compared to both *rai1 +/fh370,* B, and *rai1 fh370/fh370*, C, embryos taken at 96 hpf.

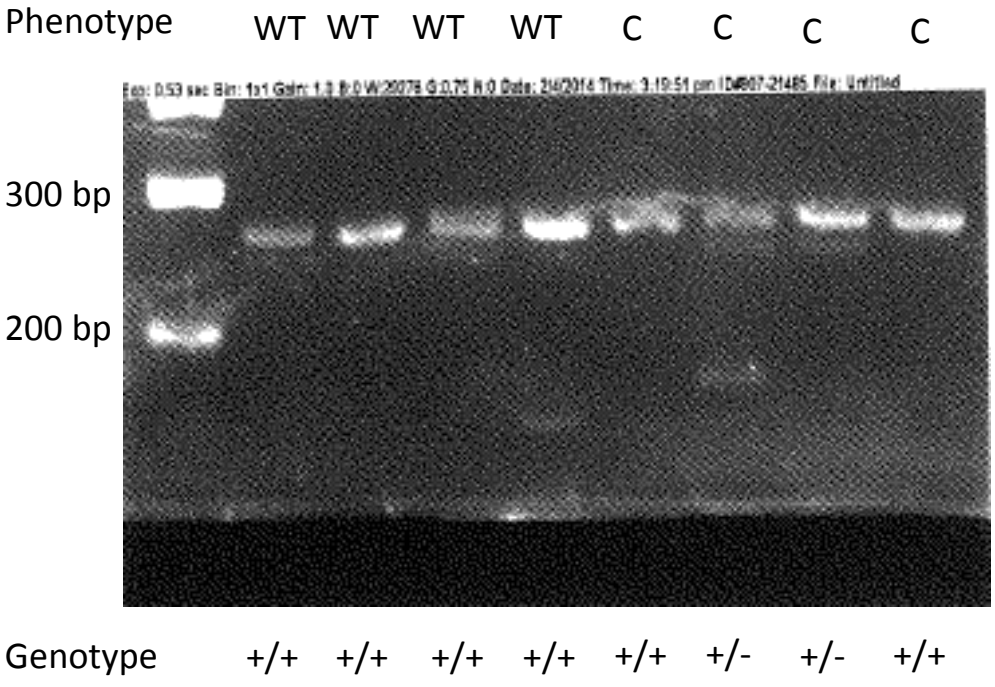

Figure 32. Agarose gel showing genotyping results for 8 *rai1 +/rh370* intercross embryos for the curved phenotype. The bottom row labels each lane of one embryo based on observed phenotype, WT for wild type and C for curved phenotype. The top row labels the lanes of the genotype found. Two bands found that are smaller than 200 bp are nonspecific amplification.

bdnf ISH

In situ hybridization of intercross larvae was conducted to examine the expression of a known target of *rai1*, *bdnf.* Images were taken of the larvae at 48 (Figure 33) and 72 hpf (Figure 34). At each time point, *bdnf* expression doesn't appear to be significantly affected, in overall level or pattern. It must be noted, that in the 48 hpf *bdnf* ISH, there appears to be reduced *bdnf* expression in the *rai1 +/fh370* embryos. This reduction of *bdnf* expression is most like attributed to the ISH procedure itself and not due to genotype, as both the wild type and homozygous mutant embryos present similar *bdnf* expression patterns and levels of expression. Within the 48 hpf cohort, *bdnf* expression was found anterior of the forebrain in all *rai1* genotypes (Figure 33). In the 72 hpf cohort, *bdnf* expression was found to be within the forebrain and midbrain regions in all *rai1* genotypes (Figure 34).

Immunostaining

Immunostaining was conducted on *rai1 +/fh370* x neuroD:GFP larvae at 72 hpf using antibodies to boost the GFP signal , by which we could observe neural development amongst the three *rai1* genotypes (Figure 35). GFP expression was found to be posterior of the developing eye (indicated by an arrow) in all *rai1* genotypes (A) *rai1* +/+, (B) +/*fh370*, and (C) (*fh370/fh370*) (Figure 35).

Additional immunostaining was conducted *rai1 +/fh370* x neuroD:GFP larvae at 72 hpf using antibodies for zn-8, a mouse anti-neurolin antibody, to observe neural development amongst the three *rai1*genotypes. (Kim et al. 2008). An anti-neurolin antibody was used because neurolin is known to play a role in motor axon growth and guidance during zebrafish development (Ott et al. 2001) zn-8 expression was similar amongst the (A) +/+, (B) +/*fh370*, and

(C) *fh370/fh370* larvae , as all genotypes showed a similar development of a CNS posterior of the hindbrain (indicated by an arrow) (Figure 36).

Altered Mendelian ratios

While a morphological phenotype was not seen amongst all genotypes of the *rai1 +/fh370* intercross larvae, the Mendelian ratios observed were not similar to the ratios that were expected. The observed Mendelian ratio from genotyped adult progeny of *rai1 +/fh370* intercrosses was: 37/70 +/+ (53%); 30/70 were +/*fh370* (43%); and 3/70 were *fh370/fh370* (4%). As for genotyped larvae used for the ISH, and immunohistochemical studies: 102/129 were +/+ (79%); 20/129 were +/*fh370* (16%); and 7/129 were *fh370/fh370* (5%). After combining the two sets of genotyping ratios we found that: 139/199 genotyped embryos were +/+ (70%); 50/199 were +/*fh370* (25%); and 10/199 were *fh370/fh370* (5%). As shown by the genotyping data, there is clear evidence that the observed ratios have deviated significantly from the expected 25:50:25 Mendelian ratios. A Chi Square test was conducted on the 3 genotypes with two degrees of freedom, finding that for a test with df=2, the $\chi^2 = 216.4975$ with a P-value < 0.00001, which is significant. While these data provide evidence for a significant deviation from Mendelian genotypic ratios; however, upon further inspection of the genotyped larvae used for the ISH and immunnohistochemical studies, only 5% of the embryos were homozygous mutants and 79% were wild type. These ratios may have likely been due to inadvertent matings of wild type and heterozygous *rai1* fish, thus boosting the number of wild type embryos genotyped. So further genotyping must be taken to ensure there is an actual deviation from the expected Mendelian ratios.

A

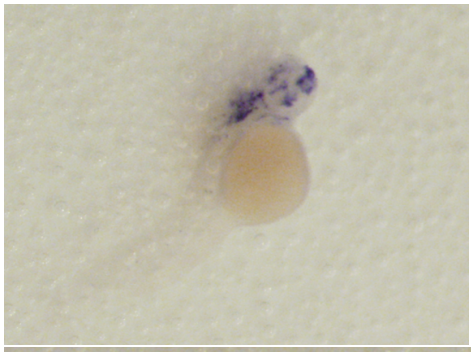

B

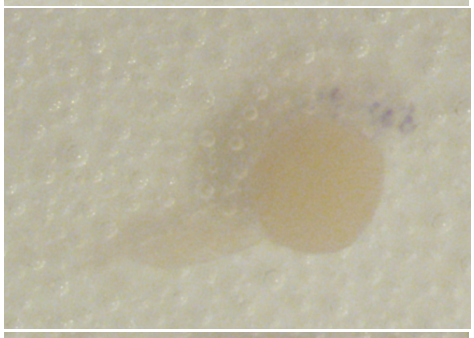

C

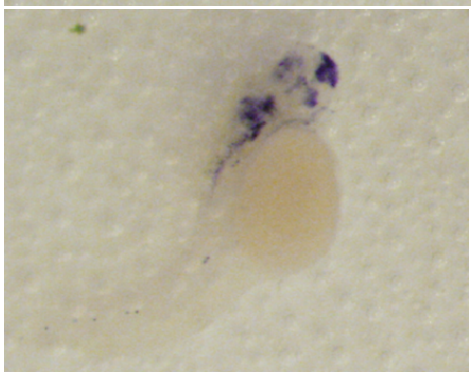

Figure 33. Images of ISH of 48 hpf *rai1 +/rh370* intercross larvae probed for *bdnf*. 48 hpf *rai1* +/+ larvae (A) probed for *bdnf* show normal expression (ZFIN); furthermore, *fh370/fh370* larvae (C) exhibited the same normal *bdnf* expression (ZFIN) as the wild type. *bdnf* expression doesn't seem to be affected by *rai1* genotype as wild type and *rai1 -/-* embryos show similar *bdnf* expression pattern and level. The *rai1+/-* embryos showed minor expression but not in the same level as +/+ and -/-, which most likely is attributed to the ISH procedure itself.

A

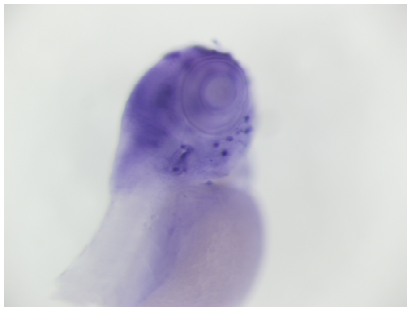

B

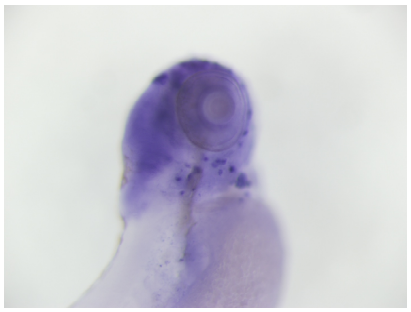

C

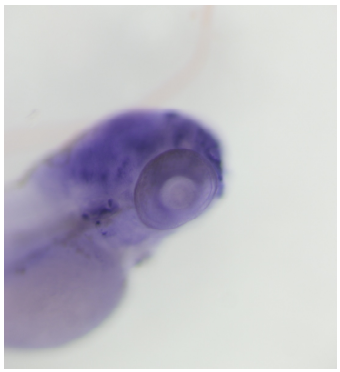

Figure 34. Images of ISH of 72 hpf *rai1 +/rh370* intercross larvae probed for *bdnf*. 72 hpf *rai1* +/+ (A) larvae probed for *bdnf* show normal expression (ZFIN); furthermore, +/*fh370* (B) and *fh370/fh370* (C) larvae exhibited the same normal *bdnf* expression (ZFIN) as the wild type. *bdnf* expression within the cohorts does not depend on the *rai1* genotype.

A

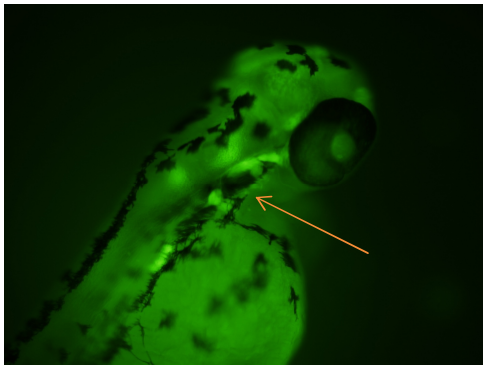

B

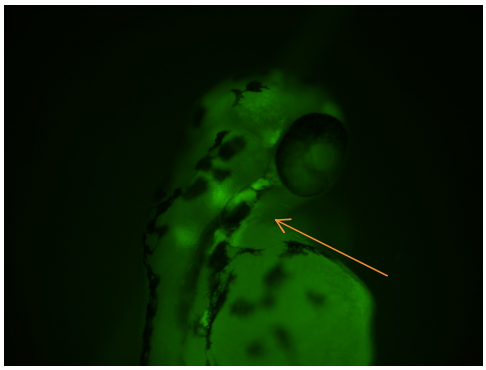

C

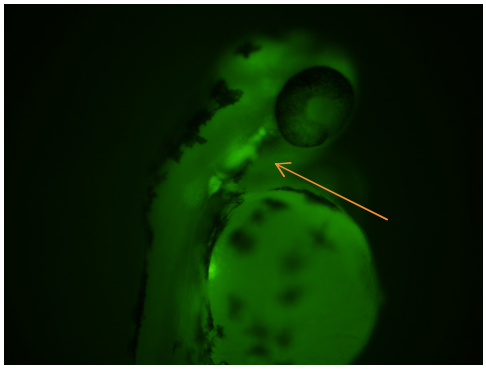

Figure 35. Images of immunostaining for GFP in *rai1 +/fh370* x neuroD:GFP larvae. GFP expression is localized in the same location (indicated by an arrow) for *rai1* (A) +/+, (B) +/*fh370*, and (C) *fh370/fh370*. *rai1* genotype had no effect on GFP expression. NeuroD:GFP typically is observed in the posterior lateral line neuromasts which is consistant with the highlight regions indicated by arrows (ZFIN).

A

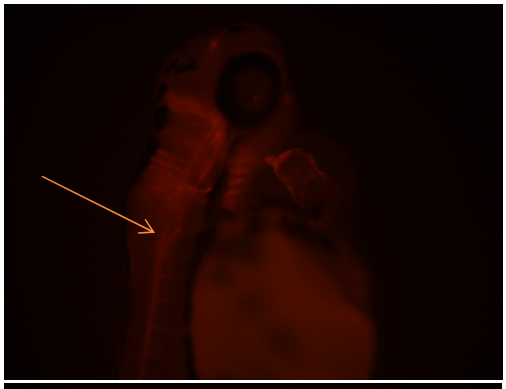

B

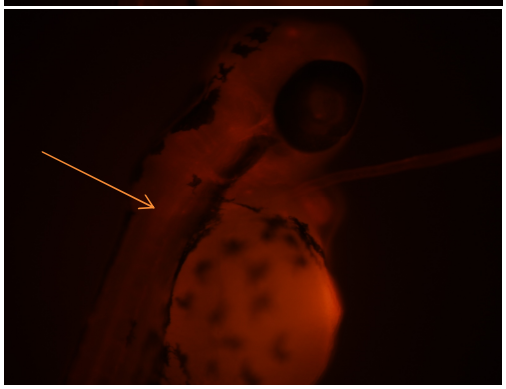

C

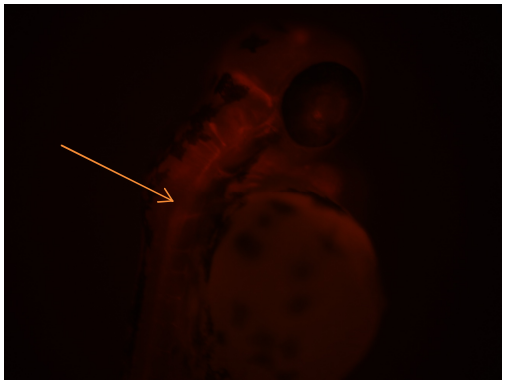

Figure 36. Images of immunostaining for zn-8 in *rai1 +/fh370* x neuroD:GFP larvae. Zn-8 expression is seen through the brain and in the same location for *rai1* (A) +/+, (B) +/*fh370*, and (C) *fh370/fh370.* Development of a CNS down the back (indicated by an arrow) is visible in all three genotypes. Zn-8, or anti-neurolin is used because neurolin is known to play a role in motor axon growth and guidance during zebrafish development

Discussion

No presence of morphological phenotypes in MO injected larvae.

MO injected embryos did not present a morphological phenotype in the larvae. As for the 10 mg *rai1* MO injected embryos with the forebrain necrosis, the necrosis was reduced when the same embryos were observed again at 48 hpf. This phenotype is most likely due to the off target effects of the MO inhibiting other genes; however, more controls would be need to be observed to support this. Further development of an expression vector (containing the zebrafish rai1 protein and GFP reporter gene) along with a zebrafish rai1 antibody are needed to determine if the morpholino is reducing *rai1* expression. Overall, we cannot say for certain that the *rai1* MO does not induce a morphological phenotype, until the MO is shown to knock down protein level.

No presence of morphological phenotypes in heterozygous intercross larvae.

There was no morphological phenotype in the heterozygous *rai1 +/fh370* intercross larvae. Genotyped *rai1 +/fh370* and *rai1 fh370/fh370* embryos did not present morphological phenotypes into maturity showing that zebrafish can develop to maturity with a haploinsufficiency or complete loss of *rai1*. While a curved phenotype paired with abnormal behavior was observed in one clutch of the *rai1 +/fh370* embryos, subsequent genotyping showed the phenotypes were not linked to the *fh370* mutation. These phenotypes are most likely attributed the background of the ENU mutagenized males at the Moens TILLING Research group. ISH for *bdnf*, a known downstream target bound by rai1 (Burns et al. 2010), showed similar expression levels and locations of expression throughout all genotypes of a cohort of *rai1 +/rh370* intercross larvae. This evidence supports the notion that the *rai1* genotype of the larvae does not affect the expression levels of *bdnf*. Even further, the whole mount immunostaining observing for neural development showed similar neural development in all genotypes of *rai1*

+/*rh370* x neuroD:GFP intercross larvae. Based on the results, haploinsufficiency or complete loss of *rai1* may not induce a phenotype and may not affect neural development or the expression of at least one known downstream target involved in neural development, *bdnf* (Burns et al. 2010). Further investigation is needed with rai1 antibodies

***A rai1* deficiency during zebrafish development can be overcome, but not often.**

With the identification of several male and female *fh370/fh370* mutants, with subsequent mutation confirmation via sequencing as well as successful homozygous mutant intercrosses, one can speculate that *rai1* is not needed for later development. However, a loss of one or both copies of *rai1* puts that zebrafish at a significant disadvantage impacting survivability in the earlier developmental stages, and this is supported with the genotyping ratio data in Chapter 3. With the total number of embryos genotyped being 199, a Chi Square analysis was conducted for the three genotypes with two degrees of freedom. We found that $\chi^2 = 216.4975$ with a P-value < 0.00001, which rejects the hypothesis that the observed genotype ratios are similar to the expected Mendelian genotype ratios. So while there are *fh370/fh370* zebrafish that have survived to reproduce, overcoming the fitness disadvantage caused by the deficiency of *rai1* may prove difficult in the earlier stages of development. In all, *rai1* deficiency is not a genetic lethal, but significantly reduces survivability in zebrafish. With that being said, it must also be noted that the genotyping assay is not always 100% reliable and the chance for inaccuracies in genotyping are possible.

CHAPTER 4: Altered *rai1* expression in response to drug treatments

Introduction

Previous Research

Vyas investigated the role of retinoic acid (RA) and 4-diethylaminobenzaldehyde (DEAB) on *rai1* expression in zebrafish embryos (2009). DEAB inhibits the synthesis of RA by inhibiting the oxidizing function of retinaldehyde dehydrogenase (Begemann et al. 2004; Russo et al. 1988). Vyas used various dosages of RA and DEAB treatment both individually and together on various embryonic stages of development. Vyas concluded that RA was not solely responsible for *rai1* expression. Vyas' experimental setup called for RA/DEAB/RA&DEAB treatments to be given at one time point, 8 hpf, or in the case of one cohort, 8 and 27 hpf. Evaluation of *rai1* expression in zebrafish embryos treated with RA/DEAB/Dimethylsulfoxide (DMSO) at other times in zebrafish development has not been done yet. I propose to evaluate

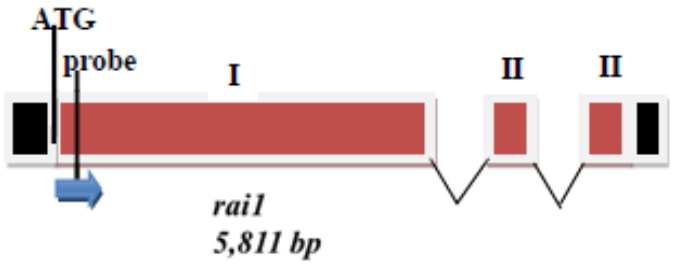

Figure 37. Schematic presentation of *rai1* probe used by Vyas. The probe hybridizes to the 5' end of exon 1 of the *rai1* gene (498 bp long).

Source: **(Vyas 2009)**

zebrafish *rai1* expression of embryos treated with RA/DMSO/DEAB 2 hours before different fixation times using the same probe that Vyas used in her experiments (Figure 38).

Retinoic Acid

Retinoic acid, a metabolite of retinol (ROH; Vitamin A), has been shown to be vital for numerous developmental processes in various models including zebrafish and is known to be present in a spatiotemporal pattern within embryos (Begemann et al. 2004; Duester 1996; Grandel et al. 2002; Perz-Edwards et al. 2001). Conversion from ROH to RA begins with the oxidation of ROH to retinal (RAH) with alcohol dehydrogenase (ADH) (Duester 1996). RAH is subsequently oxidized by aldehyde dehydrogenase (ALDH) into retinoic acid (Duester 1996). Today this aldehyde dehydrogenase is known as retinaldehyde dehydrogenase (raldh) (Begemann et al. 2004; Grandel et al. 2002; Perz-Edwards et al. 2001).There are three retinaldehyde dehydrogenase genes (*raldh1, raldh2, raldh3*) expressed in specific locations within vertebrate embryos, including zebrafish (Grandel et al. 2002). RA has a significant role in the development of the central nervous system (CNS) as well as key developmental processes as early as gastrulation (Begemann et al. 2004; Grandel et al. 2002). RA signaling is involved with the patterning of the anterior-posterior axis of the CNS and the induction of the pectoral fin bud (Grandel et al. 2002). The gene *retinaldehyde dehydrogenase2* (*raldh2*), known to synthesize RA from RAH, is expressed during gastrulation in the involuting mesoderm as well as during later stages of embryogenesis in branchial arches, fin buds, and paraxial mesoderm (Grandel et al. 2002).

4-diethylaminobenzaldehyde

DEAB inhibits the synthesis of RA by inhibiting the oxidizing function of retinaldehyde dehydrogenase (Begemann et al. 2004; Russo et al. 1988). DEAB has been used extensively for the purposes of studying development when RA synthesis has been inhibited (Begemann et al. 2002; Russo et al.; Perz-Edwards et al. 2001). DEAB treatments of zebrafish embryos during gastrulation affects the anteroposterior distribution of branchiomotor neurons in the posterior nuclei, mimicking the embryonic effects of ROH deprivation or targeted disruption of *raldh2* (Begemann et al. 2004; Perz Edwards et al. 2001). DEAB treatment after gastrulation reduces the number of branchiomotor neurons in the vagal nucleus (Begemann et al. 2004).

Aims

- We hypothesize that there will be increased expression of *rai1* by following treatment with RA in all of the time points tested as detected by the ISH.
    - We will investigate if RA induces the expression of *rai1* during embryogenesis at various time points.
- We hypothesize that DEAB will decrease expression of *rai1* at all developmental time points, while DMSO drug treatment will not increase or decrease *rai1* expression levels.
    - We will investigate if DEAB reduces *rai1* expression during embryogenesis at various time points.
    - We will investigate if DMSO impacts *rai1* expression during embryogenesis at various time points.

Materials and Methods

RA and DEAB Preparation

All-trans RA was obtained in powder form (Sigma) and RA stocks were made in ethanol at a 1 mM concentration. Part of the stock was diluted 1:5 with DMSO making the concentration 200 μM. The 200 μM RA dilution was further diluted 1:50 with DMSO making the concentration 4 μM. 10 μl of this 4 μM stock is then added to 20 ml of embryo medium to make the final concentration 2 nM. DEAB (Sigma) stocks were made in ethanol at a 100 mM concentration. Part of the stock was diluted 1:10 with DMSO to make a concentration of 10 mM. 10 μl of this 10 mM stock was then added to 20 ml of embryo medium to make a final concentration of 5 μM. 10 μl of DMSO was added to the no drug control dish.

Embryo Cultivation

Embryos were harvested and collected as described in Chapter 2. In addition to the drugs specified about, each dish received 500 μl of 0.12% of 1-phenyl-2-thiourea (PTU) to inhibit embryo pigmentation.

Experimental Setup

Each time point contained three cohorts of 40 embryos. Each cohort was treated with either RA, DEAB or DMSO at 16, 19, 25, and 28 hpf. 54 hpf embryos only received the DMSO and DEAB treatments as we reasoned there would be enough endogenous RA production at that stage that DEAB would have a minimal effect. The embryos were placed back in the 28.5ºC incubator and allowed to develop for two more hours, after which they were dechorionated and fixed at 18, 21, 27, 30, and 56 hpf. For clarity, this experiment was performed only one time.

***In Situ* Hybridization**

ISH followed the same protocols that are found in Chapter Two. The treatment cohorts at each time point were probed for either *rai1*, *cyp26a1*(Abu-Abed et al. 2001), which is known to be up-regulated in the presence of RA, and *krox20* (Morriss-Kay et al. 1991) in 18 hpf embryos as its expression is altered in the presence of excess RA levels .

Results

18 hpf embryos treated with DMSO showed the greatest *rai1* expression

The 18 hpf embryos treated with DEAB showed reduced expression of *rai1* as shown in Figure 38A. Furthermore, we see increased expression in the hindbrain and end of the tail in the RA treated embryos (Figure 38C). Most notably, the 18 hpf embryo cohort treated with DMSO showed the real level of *rai1*expresssion found in forebrain, hindbrain, and some areas of the chorion when embryos are not treated with RA or DEAB (Figure 38B).

27 hpf embryos treated with RA showed the greatest *rai1* expression

Within the 27 hpf embryo cohort, *rai1* expression decreased in the presence of DEAB (Figure 39A). For RA treated embryos, there is significantly increased *rai1* expression, which can be seen in the forebrain and in the tail (Figure 39C). Finally in the DMSO treated embryos, there was a small amount of background in the yolk sac, but overall nothing significant (Figure 39B).

A

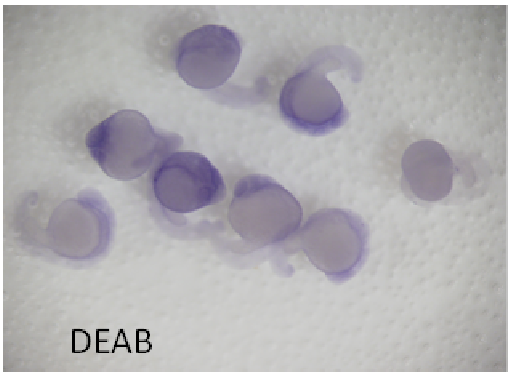

B

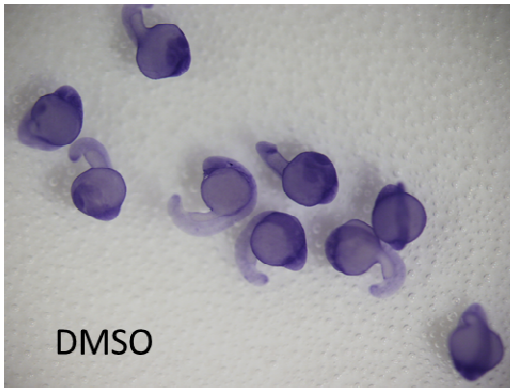

C

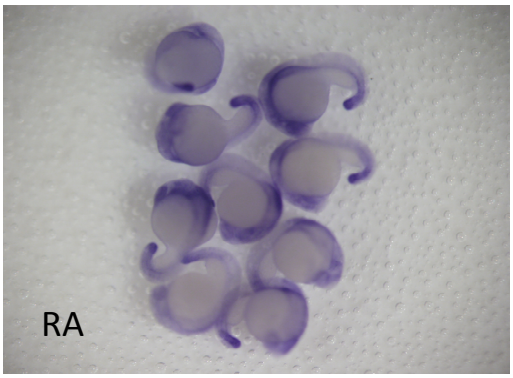

Figure 38. ISH 18 hpf embryos showing *rai1* expression in response to drug treatments. A, embryos treated with DEAB show reduced *rai1* expression; B, DMSO treated embryos show the most *rai1* expression of the three cohorts; C, RA treated embryos show less *rai1* expression than DMSO treated embryos.

A

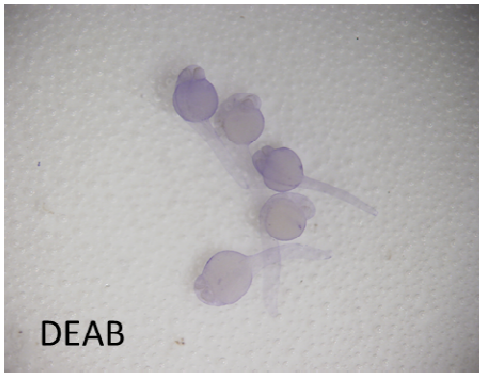

B

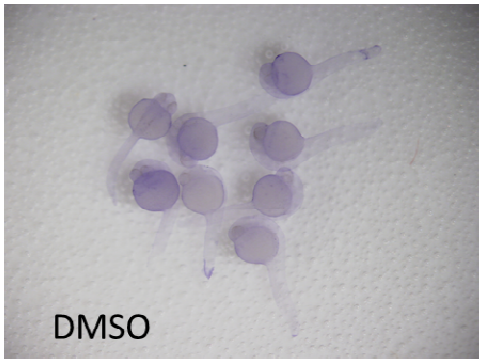

C

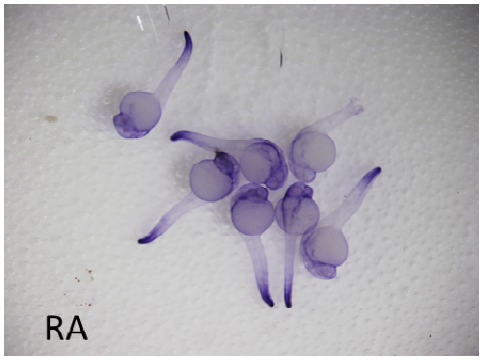

Figure 39. ISH 27 hpf embryos showing *rai1* expression in response to drug treatments. A, embryos treated with DEAB show reduced *rai1* expression; B, DMSO treated embryos show less *rai1* expression than RA treated embryos; C, RA treated embryos show the most *rai1* expression of the three cohorts in the neural and tail cells.

Drug treatments have no impact on *rai1* expression in 56 hpf embryos

In the 56 hpf embryo cohort, *rai1* expression was equal in DMSO and RA treated embryos when comparing the two treatment groups (Figure 40A & B). The probe for cyp26a1 showed that the RA drug treatments were in fact working all the way through 56 hpf (Figure 41A & B). *Krox20* showed increased expression in 18 hpf embryos. Images from 21 and 30 hpf cohorts as well as other cohort *cyp26a1* and *krox20* images were not shown.

Discussion

25 hpf may be a key time point in which *rai1* expression can be influenced

The ISH of the embryos in the 27 hpf cohort showed increased expression of *rai1* in the forebrain of the embryo when compared to DMSO and DEAB treatment groups. The 18, 21, and 30 hpf embryo cohorts did not show increased *rai1* expression when comparing the RA treated embryos of each time point cohort to the DEAB and DMSO treated embryos. *Krox20* showed increased expression in 18 hpf embryos, and this is consistent with previous data (Morris-Kay et al. 1991). The 56 hpf embryo cohort did not show increased *rai1* expression when compared to the DMSO treatment group. The evidence shown by the 27 hpf may support the notion that *rai1* expression in zebrafish is more affected by RA or DEAB treatments between 25 and 27 hpf than other times during zebrafish development. This may be a developmental time that could be further investigated to elucidate how and why RA treatments affect *rai1* expression here more than other time points. Especially when at 25 hpf, the embryo is in the process of forming primary body organs such as the brain, retina, and inner ear.

These results are in stark contrast to the findings of Vyas in 2009. Vyas found that RA induced a greater amount of expression after 24 hpf, while here RA had reduced expression in 56

hpf embryos. Vyas also observed cases of reduced *rai1* expression in the presence of DEAB and DMSO, these results show an increase of *rai1* expression in the presence of DMSO and DEAB compared to RA. Furthermore, we found that DEAB did not induce a morphological phenotype as compared to the findings of Vyas (2009). Repeated experiments are necessary to verify these findings.

A

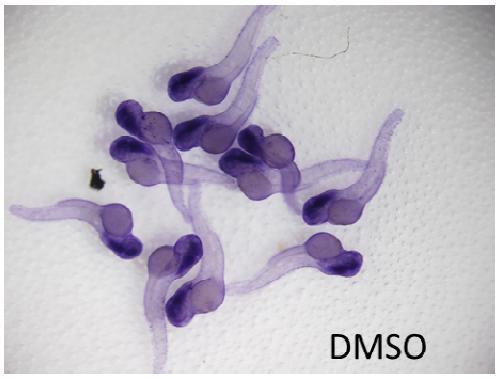

B

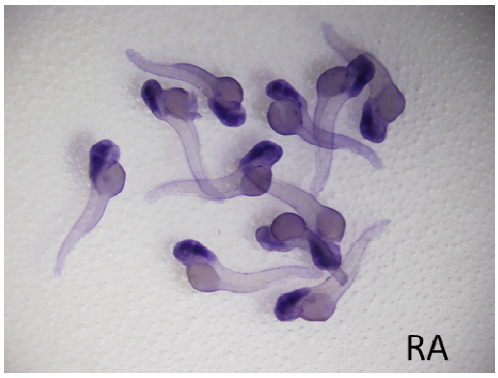

Figure 40. ISH 56 hpf embryos showing *rai1* expression in response to drug treatments. Embryos treated with DMSO (A) showed equal *rai1* expression as RA treated embryos (B).

A

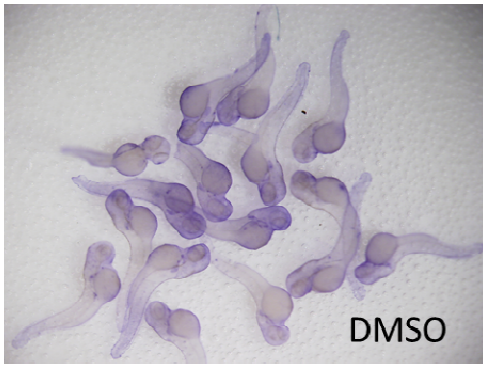

B

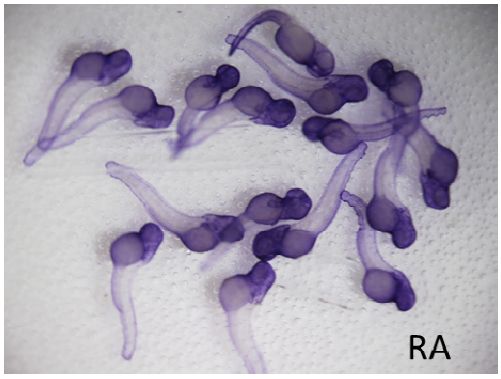

Figure 41. ISH 56 hpf embryos showing cyp26a1 expression in response to drug treatments. Embryos treated with DMSO (A) show lower *cyp26a1* expression when compared to RA treated embryos (B).

CHAPTER 5: Future Directions

Since *rai1* is expressed as early as 2 hpf in zebrafish, it would be vitally important to quantify the *rai1* expression with shorter intervals between time points, such as starting at 0 hpf and testing every hour or even every 30 minutes using the advantage of 96 wells. Allowing us to test at the hour or even 30 minute intervals would provide a more accurate picture of when *rai1* expression increases and decreases through embryogenesis.

The MO study found no long-term lethal morphological phenotype, and more controls should be used to ensure *rai1* is being knocked down in the embryo. We can do this in two ways. One way would be to develop a zebrafish rai1 antibody and use that to measure protein expression in the embryo. Another way would be to create a reporter vector and attach GFP to a sequence targeted by the MO. This would allow you to ensure there is *rai1* knockdown by the MO.

After finding that both males and females can grow and reproduce without any copies of *rai1* with wild type fish, the first measure that should be taken is to obtain more homozygous *rai1* mutants (male and female) and try to mate them. This will show that *rai1* is not essential for growth and eventually reproduction in zebrafish, even between two homozygous mutants. Furthermore, we can use identified homozygous females to observe whether maternal *rai1* expression is involved with normal zebrafish embryogenesis.

While a morphological phenotype was not found in either the *rai1 +/rh370* mutants or the *rai1*MO injected Zirc AB fish, the behavior phenotype has not been fully investigated. It has been found that melatonin induces a sleep-like state in zebrafish (Zhdanova et al. 2001). SMS patients have an inverted circadian rhythm and as such, a potential investigation would be to use the same techniques that Cahill and his team used to investigate circadian rhythmicity in locomotor activity in larval zebrafish (1998). A direction to investigate would be the locomotor activity of offspring from *rai1 +/rh370* and if possible *rai1 rh370/rh370* mutant adults with regards to the natural circadian rhythm. We would cross *rai1 +/rh370* and if possible *rai1 rh370/rh370* mutant adults to obtain an array of genotypes including a haploinsufficiency and complete loss of *rai1*. Following a 10 day growth period, fish were individually housed in 100 cylindrical wells drilled in a 10X10 grid in a 1.2 cm thick specimen plate made of translucent white polyethylene (Cahill et al. 1998). We will use a diffuse axial illuminator placed above the providing infrared (>700 nm) illumination, with backlighting provided by a mirror placed under the samples. A series of 60 images (1/second) will be collected every 4-5 minutes and data collection would be done by Optimas image analysis software. Image collection would occur at night and would be compared to a control zebrafish group.

After initially finding increased *rai1*, there were issues in subsequent attempts to recapitulate the results for the 27 hpf embryos. Repeating the ISH is tantamount to providing further support to the results found in the drug treatment study; furthermore, other time points should evaluated, and maybe lengthening the time the drug treatment is in the embryo medium with embryos may affect expression as well. To do this, one could do various amounts of times of drug treatment for embryos and fix all cohorts at a single developmental time point, then conduct ISH for comparison.

Finally, finishing development of the overexpression vector to inject into 1 cell stage Zirc AB embryos is vital to understanding if an overexpression of *rai1* can induces a morphological phenotype in wildtype zebrafish. Continued adult genotyping must occur to elucidate if there are altered Mendelian ratios, with this data, one could find if zebrafish truly need *rai1* at early stages of development.

Literature Cited

Abu-Abed S, Dolle P, Metzger D et al. (2001) The retinoic acid-metabolizing enzyme, CYP26A1, is essential for normal hindbrain patterning, vertebral identity, and development of posterior structures. *Genes Dev* 15: 226 – 240.

Allanson JE, Greenberg, and Smith ACM. (1999) The face of Smith-Magenis syndrome: a subjective and objective study. *J Med Genet* 26: 394 – 397.

Andrew SE, Goldberg YP, Kremer B et al. (1993) The relationship between trinucleotide (CAG) repeat length and clinical features of Huntington's disease. *Nature Genet* 4: 398 – 403.

Barnicoat AJ, Moller HU, Palmer RW et al. (1996) An unusual presentation of Smith – Magenis syndrome with iris dysgenesis. *Clinical Dysmorphology* 5:153 – 158.

Bax C and Zies DL. (2011) Determination of specific rai1 binding sites. *The FASEB J* 25(1): 698.2

Begemann G, Marx M, Mebus K et al. (2004) Beyond the neckless phenotype: influence of reduced retinoic acid signaling on motor neuron development in the zebrafish hindbrain. *Developmental Biology* 271: 119 – 129.

Beunders G, Voorhoeve E, Golzio C et al. (2013) Exonic deletions in AUTS2 cause a syndromic form of intellectual disability and suggest a critical role for the C terminus. *Am J of Hum Genet* 92: 210 – 220.

Bi W, Saifi GM, Shaw CJ et al. (2004) Mutations of RAI1, a PHD-containing protein, in nondeletion patients with Smith – Magenis syndrome. *Hum Genet* 115: 515 – 524.

Bi W, Ohyama T, Nakamura et al. (2005) Inactivation of *Rai1* in mice recapitulates phenotypes observed in chromosome engineered mouse models for Smith – Magenis syndrome. *Hum Mol Genet* 14(8): 983 – 995.

Bienz M. (2005) The PHD finger, a nuclear protein-interaction domain. *TRENDS in Biochemical Sciences* 31(1): 35 – 40.

Burns B, Schmidt K, Williams SR et al. (2010) Rai1 haploinsufficiency causes reduced bdnf expression resulting in hyperphagia, obesity and altered fat distribution in mice and humans with no evidence of metabolic syndrome. *Hum Mol Genet* 19(20): 4026 – 4042.

Cahill GM, Hurd MW, and Batchelor MM. (1998) Circadian rhythmicity in the locomotor activity of larval zebrafish. *NeuroReport* 9: 3445 – 3449.

Carmona-Mora P, Canales CP, Cao L et al. (2012) RAI1 transcription factor activity is impaired in mutants associated with smith – magenis syndrome. *PLOS ONE* 7(9): e45155.

Carmona-Mora P and Walz K. (2010) Retinoic acid induced 1, RAI1: a dosage sensitive gene related to neurobehavioral alterations including autistic behavior. *Current Genomics* 11: 607 – 617.

Chen RM, Lupski JR, Greenberg F et al. (1996) Ophthalmic manifestations of smith-magenis syndrome. *Ophthalmology* 103:1084 – 1091.

DeLeersnyder H, de Blois MC, Claustrat B et al. (2001) Inversion of the circadian rhythm of melatonin in the smith – magenis syndrome. *J of Pediatr* 139: 111 – 116.

DeLeersnyder H, de Blois, Vekemans M et al. (2001) β_1-adrenergic antagonists improve sleep and behvioural disturbances in a circadian disorder, smith-magenis syndrome. *J. of Med Genet* 38: 586 – 590.

DeLeersnyder H. (2006) Inverted rhythm of melatonin secretion in smith-magenis syndrome: from symptoms to treatment. *Trends in Endocrinology and Metabolism* 17(7): 291 – 298.

Deuster G. (1996) Involvement of alcohol dehydrogenase, short-chain dehydrogenase/reductase, aldehyde dehydrogenase, and cytochrome P450 in the control of retinoid signaling by activation of retinoic acid synthesis. *Biochemistry* 35(38): 12221 – 12227.

Draper BW, Morcos PA, and Kimmel CB. (2001). Inhibition of zebrafish *fgf8* pre-mrna splicing with morpholino oligos: a quantifiable method for gene knockdown. *Genesis* 30: 154 – 156.

Edelman EA, Girirajan S, Finucane B et al. (2007) Gender, genotype, and phenotype differences in Smith-Mmagenis syndrome: a meta-analysis of 105 cases. *Clin Genet* 71: 540 – 550.

Elsea SH, Williams SR. (2011) Smith-Magenis syndrome: haploinsufficiency of *RAI1* results in altered gene regulation in neurological and metabolic pathways. *Expert Rev. Mol. Med.* **13**(4): 1 – 14.

Elsea SH, Girirajan S. (2008) Smith-Magenis syndrome. *Eur J Hum Genet* **16**(4):412-21.

Ercan-Senciek AG, Davis Wright NR, Frost SJ et al. (2012) Searching for potocki-lupski syndrome phenotype: a patient with language impairment and no autism. *Brain & Development* 34(2012): 700 – 703.

Finucane BM and Jaeger ER. (1997) Smith – Magenis syndrome [letter]. *Ophthalmology* 104(5):732 – 733.

Finucane BM, Jaeger ER, Kurtz MB et al. (1993) Eye abnormalities in the Smith – Magenis contiguous gene deletion syndrome. *Am. J. Med. Gen.* 45:443 – 446.

Girirajan S, Elsas II LJ, Devriendt K et al. (2005) RAI1 variations in Smith – Magenis syndrome patients without 17p11.2 deletions. *J Med Genet* 42: 820 – 828.

Girirajan S, Vlangos CN, Szomju BB et al. (2006) Genotype-phenotype correlation in Smith-Magenis syndrome: evidence that multiple genes in 17p11.2 contribute to the clinical spectrum. *Genet Med* 8(7): 417 – 427.

Gomez-Pinilla F, Ying Z, Roy RR et al. (2002) Voluntary exercise induces a bdnf-mediated mechanism that promotes neuroplasticity. *J Neurophysiol* 88: 2187 – 2195.

Grandel H, Lun K, Rauch GJ et al. (2002) Retinoic acid signaling in the zebrafish embryo is necessary during pre-segmentation stages to pattern the anterior-posterior axis of the CNS and to induce a pectoral fin bud. *Development* 129: 2851 – 2865.

Greco D, Romano C, Reitano S. (2008) The new patients with dup(17)(p11.2p11.2) without autism. *Clin Genet* 73: 294 – 296.

Greenberg F, Lewis RA, Potocki L et al. (1996). Multi-disciplinary clinical study of Smith-Magenis syndrome (deletion 17p11.2). *Am J Med Genet* 62:247 – 254.

Henderson CE. (1996) Role of neurotrophic factors in neuronal development. *Current Opinion in Neurobiology* 6: 64 – 70.

Imai Y, Suzuki Y, Matsui T et al. (1995) Cloning of a retinoic acid-induced gene, GT1, in the embryonal carcinoma cell line P19: neuron-specific expression in the mouse brain. *Molecular Brain Research* (31): 1 – 9.

Itoh M, Hayashi M, Hasegawa T. (2004). Systemic growth hormone corrects sleep disturbance in Smith – Magenis syndrome. *Brain & Development* 26(2004): 484 – 486.

Kim H, Shin J, Kim S et al. (2008) Notch-regulated oligodendrocyte specification from radial glia in the spinal cord of zebrafish embryos. *Developmental Dynamics* 237: 2081 – 2089.

Kimmel CB, Ballard WW, Kimmel SR et al. (1995) Stages of embryonic development of the zebrafish. *Developmental Dynamics* 203: 253 – 310.

Kirek M, Knijenburg J, White SJ, Rosenberg C et al. (2007) Diagnosis of genetic abnormalities in developmentally delayed patients: a new strategy combining MLPA and array-CGH. Am J Med Genet Part A 143A:610 – 614.

Kvarnug M, Nilsson D, Lindstrand A et al. (2013) A novel intellectual disability syndrome caused by GPI anchor deficiency due to homozygous mutations in PIGT. *J Med Genet* 50: 521 – 528.

Liburd N, Ghosh M, Riazuddin S et al. (2001) Novel mutations of *MYO15A* associated with profound deafness in consanguineous families and moderately severe hearing loss in a patient with Smith-Magenis syndrome. *Hum Genet* 109: 535 – 541.

Lieschke GJ and Currie PD. (2007) Animal models of human disease: zebrafish swim into view. *Nature Reviews* 8: 353 – 367.

MarianneJensen L and Kirchoff M. (2005) Polydactyly in a boy with Smith-Magenis syndrome. *Clin Dysmorphology* 14: 189 – 190.

Milne TA, Briggs SD, Brock HW et al. (2002) MLL targets SET domain methyltransferase activity to hox gene promoters. *Molec Cell* 10: 1107 – 1117.

Morriss-Kay GM, Murphy P, Hill RE et al. (1991) Effects of retinoic acid excess on expression of hox-2.9 and krox-20 and on morphological segmentation in the hindbrain of mouse embryos. *The EMBO Journal* 10(10): 2985 – 2995.

Nakamura T, Mori, T, Tada S et al. (2002) ALL-1 is a histone methyltransferase that assembles a supercomplex of proteins involved in transcriptional regulation. *Molec Cell* 10: 1119 – 1128.

Neff MM, Neff JD, Chory J et al. (1998) dCAPS, a simple technique for the genetic analysis of single nucleotide polymorphisms: experimental applications in *Arabidopsis thaliana* genetics. *The Plant Journal* 14(3): 387 – 392.

Ott H, Diekmann H, Stuermer CAO et al. (2001) Function of neurolin (dm-grasp/sc-1) in guidance of motor axons during zebrafish development. *Developmental Biology* 235: 86 – 97.

Perz-Edwards A, Hardison NL, Linney E. (2001) Retinoic acid-mediated gene expression in transgenic reporter zebrafish. *Developmental Biology* 229: 89 – 101.

Potocki L, Glaze D, Tan DX et al. (2000A) Circadian rhythm abnormalities of melatonin in Smith – Magenis syndrome. *J Med Genet* 37: 428 – 433.

Potocki L, Chen KS, Park SS et al. (2000B) Molecular mechanism for duplication o17p11.2 – the homologous recombination reciprocal of the Smith-Magenis microdeletion. *Nature Genet* 24: 84 – 87.

Potocki L, Bi W, Treadwell-Deering D et al. (2007) Characterization of Potocki-Lupski syndrome (dup(17)(p11.2p11.2)) and delineation of a dosage-sensitive critical interval that can convey an autism phenotype. *Am J of Hum Genet* 80: 633 – 649.

Russo JE, Hauguitz D, and Hilton J. (1988) Inhibition of mouse cytosolic aldehyde dehydrogenase by 4-(diethylamino) benzaldehyde. *Biochemical Pharmacology* 37(8): 1639 – 1642.

Schuurs-Hoeijmakers JHM, Oh EC, Vissers LELM et al. (2012) Recurrent de novo mutations in PACS1 cause defective cranial-neural-crest cell migration and define a recognizable intellectual-disability syndrome. *Am J of Hum Genet* 91: 1122 – 1127.

Shelley BP and Robertson MM. (2005). The neuropsychiatry and multisystem features of the Smith – Magenis syndrome: a review. *J Neuropsychiatry Clin Neurosci* 17: 1.

Smith ACM, MacGavran L, Robinson J et al. (1986) Interstitial Deletion of (17)(p11.2p11.2) in Nine Patients. *Am J Med Genet* 24(3):393 – 414.

Soler-Alfonso C, Motil KJ, Turk CL et al. (2011) Potocki-Lupski syndrome: a microduplication syndrome associated with oropharyngeal dysphagia and failure to thrive. *J of Pediatr* 158(4): 655 – 659.

Spadoni E, Colapietro P, Bozzola M et al. (2004) Smith – Magenis syndrome and growth hormone deficiency. *Eur J Pediatr* 163: 353 – 358.

Tadros W and Lipshitz HD. (2009) The maternal-to-zygotic transition: a play in two acts. *Development* 136: 3033 – 3042.

Tahir R, Kennedy A, Elsea SH et al. (2014). Retinoic acid induced-1 (Rai1) regulated craniofacial and brain development in *Xenopus*. *Mechanisms of Development* 133: 91-104.

Tomona N, Smith ACM, Guadagnini JP et al. (2006) Craniofacial and Dental phenotype of Smith – Magenis syndrome. *Am J Med Get PartA* 140A: 2556 – 2561.

Toulouse A, Rochefort D, Roussel J. (2003) Molecular cloning and characterization of human RAI1, a gene associated with schizophrenia. *Genomics* 82(2003): 162 – 171.

Truong HT, Solaymani-Kohal S, Baker KR et al. (2008) Diagnosisng Smith – Magenis syndrome and duplication 17p11.2 syndrome by rai1 gene copy number variation using quantitative real-time PCR. *Genetic Testing*. 12(1):67 – 74.

Tsirikos AI, Baker ADL, and McClean C. (2010) Surgical treatment of scoliosis in Smith – Magenis syndrome: a case report. *J Med Case Reports* 4: 26.

Vlangos CN, Wilson M, Blancato J et al. (2005) Diagnostic FISH probes for del(17)(p11.2p11.2) associated with Smith-Magenis syndrome should contain the RAI1 gene. *Am. J. Med. Genet. A* 132A(3):278-82.

Vyas BA. (2009) Retinoic acid induced 1 gene analysis in humans and zebrafish [thesis]. Richmond (VA): Virginia Commonwealth University. p. 1 – 112.

Warga RM and Kimmel CB. (1990) Cell movements during epiboly and gastrulation in zebrafish. *Development* 108: 569 – 580.

Williams SR, Zies D, Mullegama SV et al. Smith – Magenis syndrome results in disruption of clock gene transcription and reveals an integral role for rai1 in the maintenance of circadian rhythmicity. *Am J of Hum Genet* 90: 941 – 949.

Wong SL and Roth FP. (2005) Transcriptional compensation for gene loss plays a minor role in maintaining genetic robustness in *Saccharomyces cerevisiae*. *Genetics* 171: 829 – 833.

Yamada K, Mizuno M, and Nabeshima T. (2002) Role for brain-derived neurotrophic factor in learning and memory. *Life Sciences* 70: 735 – 744.

Zhang F, Potocki L, Sampson JB et al. (2010) Identification of uncommon recurrent Potocki-Lupski syndrome-associated duplications and the distribution of rearrangement types and mechanisms in PTLS. *Am J of Hum Genet* 86: 462 – 470.

Zhdanova IV, Wang SY, Ojingwa UL et al. (2001) Melatonin promotes sleep-like state in zebrafish. *Brain Research* 903: 263 – 268.

APPENDIX

Creating the Overexpression Vector

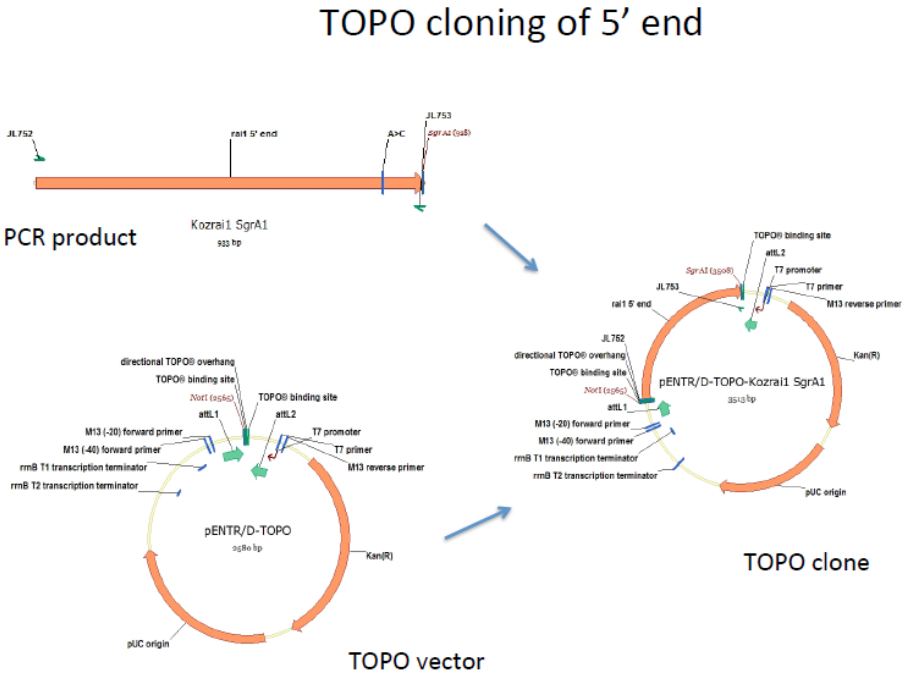

TOPO cloning of 3’ end w/o stop codon

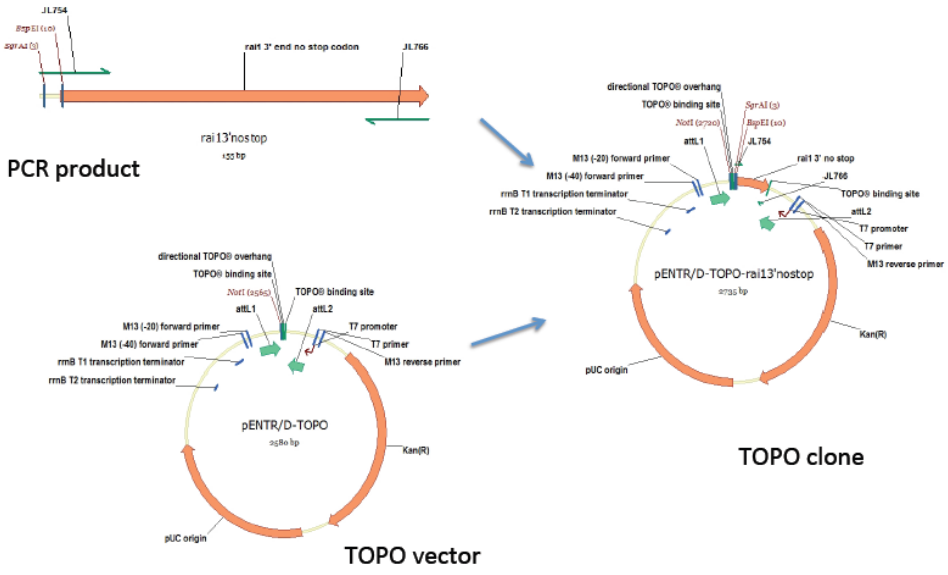

Insert 5’ end into 3’ end vector

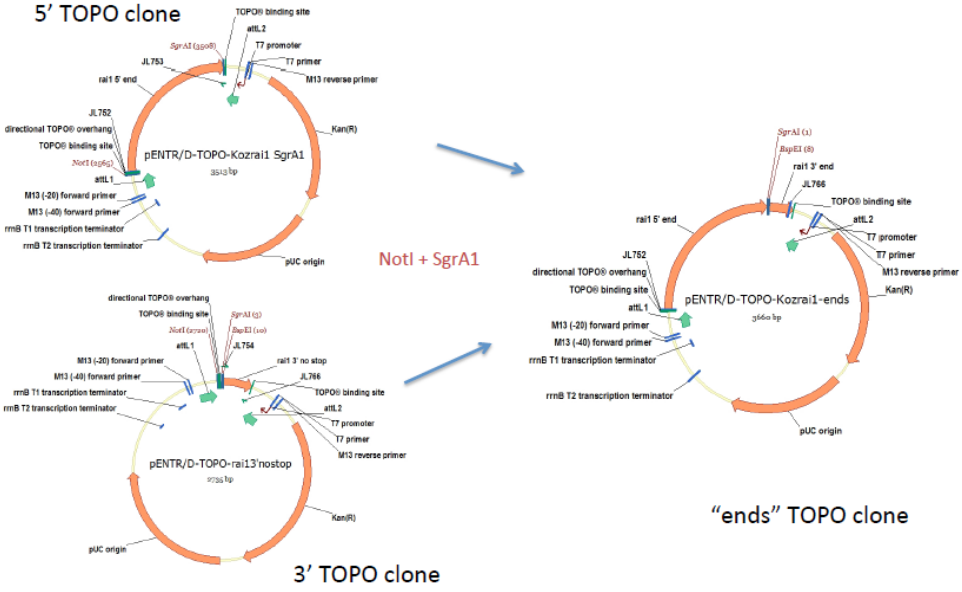

Last step: insert middle segment of *rai1*

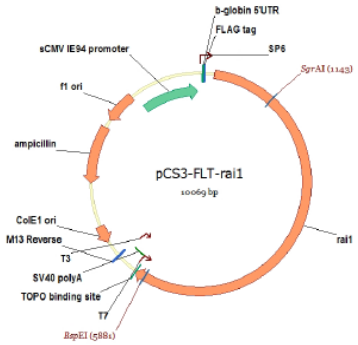

Full-length rai1 clone

SgrA1 + BspE1

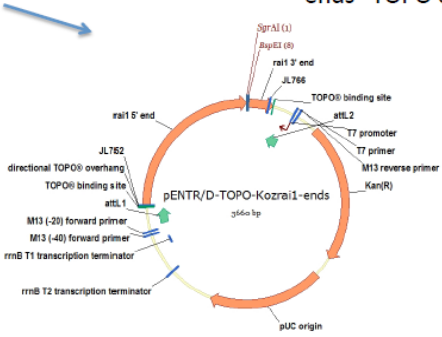

"ends" TOPO clone

Final construct, ready for Gateway cloning

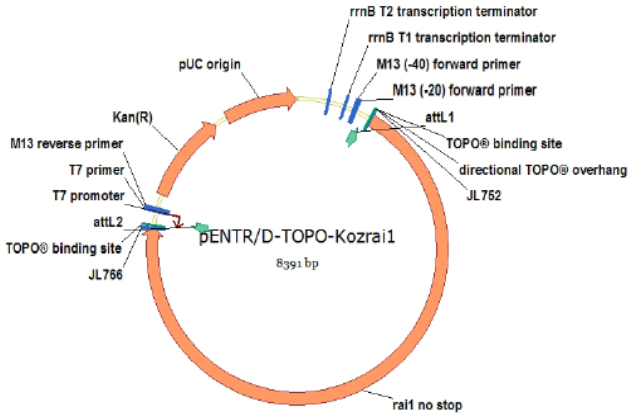

VITA

Joshua Shay Beach was born September 6, 1989 in Richmond, VA. He graduated with a Bachelor of Arts with a major in Biology from Belmont Abbey College in Belmont, NC in 2011. He joined the Human Genetics program in the Fall of 2012, and joined the laboratory of Dr. James Lister to pursue his goal of receiving further knowledge in the field of genetics.